UV-vis and Photoluminescence Spectroscopy to Understand the Coordination of Cu Cations in the Zeolite SSZ-13

Florian Göltl[1,2], Sabrina Conrad[1,3], Patrick Wolf[1,3], Philipp Müller[1], Alyssa M. Love[1], Samuel P. Burt[2], Jamie N. Wheeler[1], Robert J. Hamers[1], Kerstin Hummer[4], Georg Kresse[4], Manos Mavrikakis[2], Ive Hermans[1,2]

[1] University of Wisconsin, Madison, Department of Chemistry, University Avenue 1101, 53706 Madison, Wisconsin, USA
[2] University of Wisconsin - Madison, Department of Chemical and Biological Engineering, 1415 Engineering Drive, 53706 Madison, Wisconsin, USA
[3] Department of Chemistry and Applied Biosciences, ETH Zurich, Vladimir-Prelog-Weg 1-5, 8093 Zurich, Switzerland
[4] University of Vienna, Faculty of Physics, Computational Materials Physics, Sensengasse 8/12, 1090 Vienna, Austria
Corresponding author: fgoeltl@wisc.edu, hermans@chem.wisc.edu

Abstract:

The Cu-exchanged zeolite SSZ-13 is a highly active material in the selective catalytic reduction of nitrogen oxides and the conversion of methane to methanol. In this material a distribution of active sites is present and its characterization is a long standing challenge. In this contribution we combine molecular dynamics simulations and high-level first principles calculations to obtain accurate phase diagrams, photoabsorption and photoluminescence spectra of Cu^{I} sites in SSZ-13 and compare them to specifically designed experimental measurements. We start our analysis by using molecular dynamics and RPA calculations to calculate phase diagrams for Cu anchored in extra-framework and silanol defect sites. Subsequently we combine molecular dynamics and a time-dependent hybrid Hartree-Fock like linear response scheme to calculate photoabsorption and photoluminescence spectra. We determine that at low temperatures Cu^{I} is coordinated to multiple H_2O molecules. At elevated temperatures and low pressures all H_2O molecules desorb and Cu^{I} migrates to defect sites, as long as defects are present in the material. Theoretically predicted and experimentally measured optical spectra are in excellent agreement. Additionally we discuss the impact of defects on the observed luminescence spectra. We expect that the methods developed here will be used to better understand the distribution of Cu sites in the zeolite SSZ-13 under various conditions. Further, this work sheds light on a potential role of defects in the coordination of Cu^{I} in deNO_x-SCR in aged catalysts and helps with understanding luminescence spectra of transition metal sites in zeolites.

Introduction:

With the introduction of Cu-exchanged SSZ-13 as industrial catalyst for the selective catalytic reduction of NO_x in the presence of NH_3 in car exhaust after-treatment systems[1], interest in transition metal exchanged zeolites has been reignited. Not only are these zeolites excellent materials in deNO_x-SCR,[2,3] but they also show large promise in the direct conversion of methane to methanol,[4,5] the oligomerization of hydrocarbons[6,7] and are promising photo-emitters.[8,9] It is safe to assume that the favorable properties of these materials are closely linked to the atomic structure of the active sites. In transition metal exchanged zeolites, characterizing the atomic structure of the active sites proves to be particularly difficult, since a distribution of active sites exists[10–13] depending on the framework type, stoichiometric composition, and the synthesis and preparation of the zeolite.[14] An unambiguous characterization of the distribution of active sites, let alone the identification of the active and inactive parts of the distribution is very often not possible using only one technique. Therefore, a combination of complementary techniques is required to obtain a detailed understanding of the atomic structure of the active sites in zeolites.

Over the past few years, DFT calculations have provided significant insights into the structure of active sites in zeolite SSZ-13. Initially simple thermodynamic arguments based on static DFT calculations were used to identify the most stable Cu sites,[10,15,16] but soon it became clear that under ambient conditions several other factors influence site speciation. On one hand, a combination of molecular dynamics simulations and experimental results revealed that when Cu is directly bound to the zeolite framework, it shows a significant mobility and shifts between different local minima.[11,17,18] On the other hand, it was shown that molecules such as H_2O and NH_3 bind very strongly to the Cu monomers.[13,18–23] which leads to the formation of mobile Cu-complexes inside the zeolite pore, which are only loosely bound to the framework.[24] However, at increased temperatures or at lower gas concentrations, the coordination to the adsorbents is lost and Cu moves back into its extra framework position.[18,19,25]

To take these phenomena into account, Paolucci *et al.* calculated phase diagrams for various monomeric Cu sites in zeolite SSZ-13 and could reproduce some of the experimentally observed trends.[18] However, the calculated phase diagrams were based on the assumption that, similar to adsorption on metal surfaces, molecules only lose a fraction of their translational entropy upon adsorption to Cu.[18,26] While this relationship was shown for the adsorption of single molecules in a narrow temperature range, rigorous proof of this assumption for the adsorption of multiple molecules over a wide temperature range is still missing. Some of us therefore chose a more conservative approach and calculated phase diagrams for water adsorption using static DFT calculations and finite temperature corrections based on vibrational frequencies.[19] We furthermore used the calculated phase diagrams to assign experimentally observed IR spectra of the materials, but an unambiguous assignment of experimental features, and therefore conclusive evidence for the validity of the calculated phase diagrams, was not possible due to the inherent

complexity of the material.

As shown by the discussion above, assessing the reliability of the calculated phase diagrams is a crucial aspect for their further application and can only be achieved by directly comparing predictions to experimental results. Optical spectroscopy is a method, which, after the pioneering work of Klier *et al.* in the late 1970s and 1980s, has been used to characterize copper sites in different zeolite structures.[27,28] Today, optical spectroscopy is a routine characterization technique,[29–31] but so far only few theoretical studies have been performed in this area.[32–35] These either focused on density functional theory-based calculations, which in principle are not able to describe excited states correctly,[32,34] or used a small cluster model,[33] which neglects the complexity of the zeolite framework. Only in recent work the rapid coordination changes of Cu-cations in zeolites[11,17] have been included[35] and so far coordination changes in the presence of water[18–20,22] have been neglected in spectroscopic assignments. Furthermore, optical spectra have never been correlated to theoretically calculated phase diagrams.

In this contribution we use a combination of *ab-initio* molecular dynamics simulations and post-DFT calculations to calculate temperature dependent free energies of monovalent Cu sites anchored at extra framework positions and silanol defects in the zeolite SSZ-13. Subsequently, we use the free energies to obtain phase diagrams and calculate absorption and luminescence spectra for the most likely sites in a given temperature/pressure range. We furthermore design an experimental approach that allows for direct comparison with theoretical calculations and find excellent agreement between theory and experiment. Interestingly, we determine that Cu migrates from extra framework sites to silanol defects at high temperatures. We also discuss implications of our findings for catalysis and optical applications of transition metal exchanged zeolites.

The System:

The goal of this work is to have a fully integrated experimental and theoretical approach, which requires the detailed design of a combined experimental and theoretical strategy to provide comparability and unambiguous assignments of spectroscopic features. SSZ-13 is an ideal model-system for zeolite catalysis,[14] since it is a material in the chabazite framework (displayed in Fig. 1), which is the zeolite with the smallest primitive unit cell. Like all other zeolites it is composed of corner-sharing SiO_4-tetrahedra (T-sites). It has 12 symmetrically equivalent T-sites in the primitive unit cell, which form a double six-membered prism.[36] Substituting Si with Al activates the framework and creates a local negative charge, which is compensated for by countercations. Extra framework species can either be located in the six-ring or eight-ring (displayed in Fig. 1) and their stability is typically determined by the position of the Al atoms.[10,12,19] While the local distribution of Al can be highly complex at low Si/Al ratios, at high Si/Al ratios a majority of the Al atoms will be isolated, a situation we model here[37]. We will furthermore consider silanol defects created by substituting one Si^{4+} atom by four H^+ (d4H, displayed in

Fig. 1) or two Si atoms and an O atom by 6 H^+ (d6H, displayed in Fig. 1). Furthermore, all calculations were performed using the primitive rhombohedral unit cell, periodic boundary conditions and the Vienna Ab-Initio Simulation Package (VASP)[38,39].

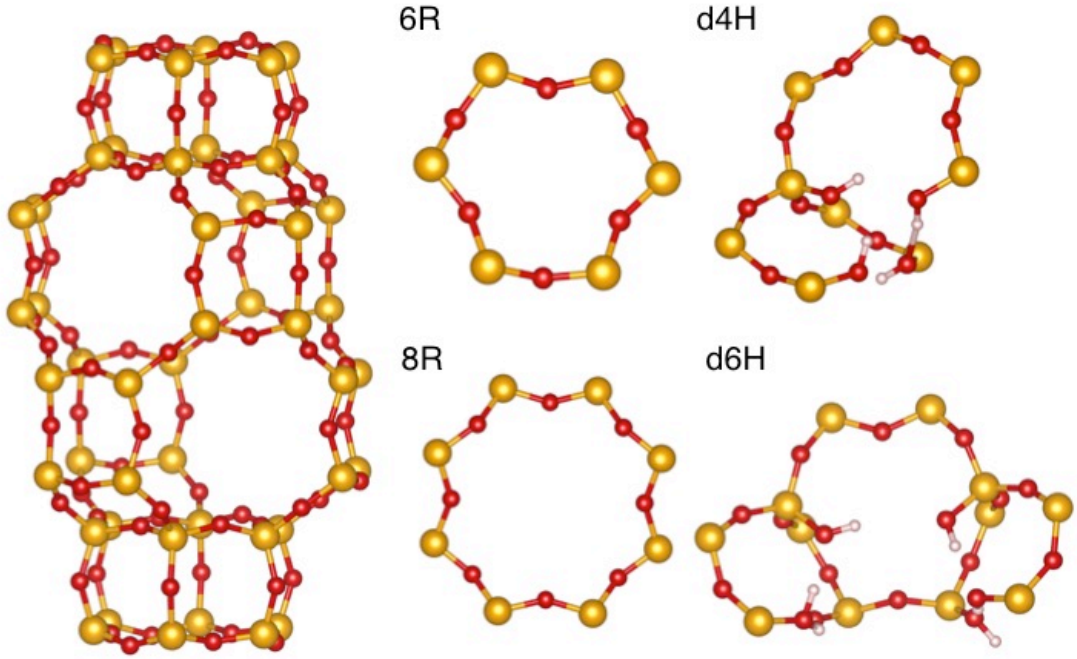

Figure 1: *The structure of SSZ-13, a zeolite in the chabazite framework, is displayed on the left hand side. In this system two different extra framework sites for Cu cations exist, one in a six-member ring (6R), shown on the right hand side at the top, and one in an eight-member ring (8R), shown in the right hand side in the middle). In our calculations we also investigate the impact of silanol defects when one Si^{4+} atom is substituted by 4 H^+ (d4H) or two Si^{4+} atoms and one O^{2-} are substituted by 6H^+ (d6H). Si atoms are displayed as yellow, O atoms as red, and H atoms as white spheres.*

Phase diagrams:

Recent work indicates that the oxidation state of Cu will depend on the exact environment, *i.e.*, the presence of different gases such as H_2O and O_2 and the temperature.[18,19,22] To calculate the phase diagram, we include Cu sites as extra framework (Cu-EF) atoms close to one Al atom and bound to the defect site with up to six adsorbed H_2O molecules located in the periodic zeolite framework. While Cu in the Cu-EF-6R and Cu-EF-8R is exchanged for H^+ and binds to activated O atoms next to Al, we exchange one to three H atoms from the single silanol (Cu-d3H-Cu-d1H) defect and one H atom from the double silanol defect (Cu-d5H) for Cu to allow for a direct bond between O and Cu. For Cu-EF-6R, Cu-EF-8R, Cu-d3H and Cu-d5H, where Cu is exchanged for one H^+, this leads to Cu^I, while Cu^{II} is formed for Cu-d2H, where two H^+ are exchanged. For Cu-d1H, where Cu is exchanged for three H^+, Cu^I and a bond between two adjacent O atoms are formed. Subsequently, we will refer to Cu in the different structures as X-mH_2O, where X stands for the type of site (*i.e.*

Cu-EF, Cu-d1H-Cu-d3H, Cu-d5H) and m stands for the number of adsorbed water molecules. All the corresponding structures are displayed in Fig. 2.

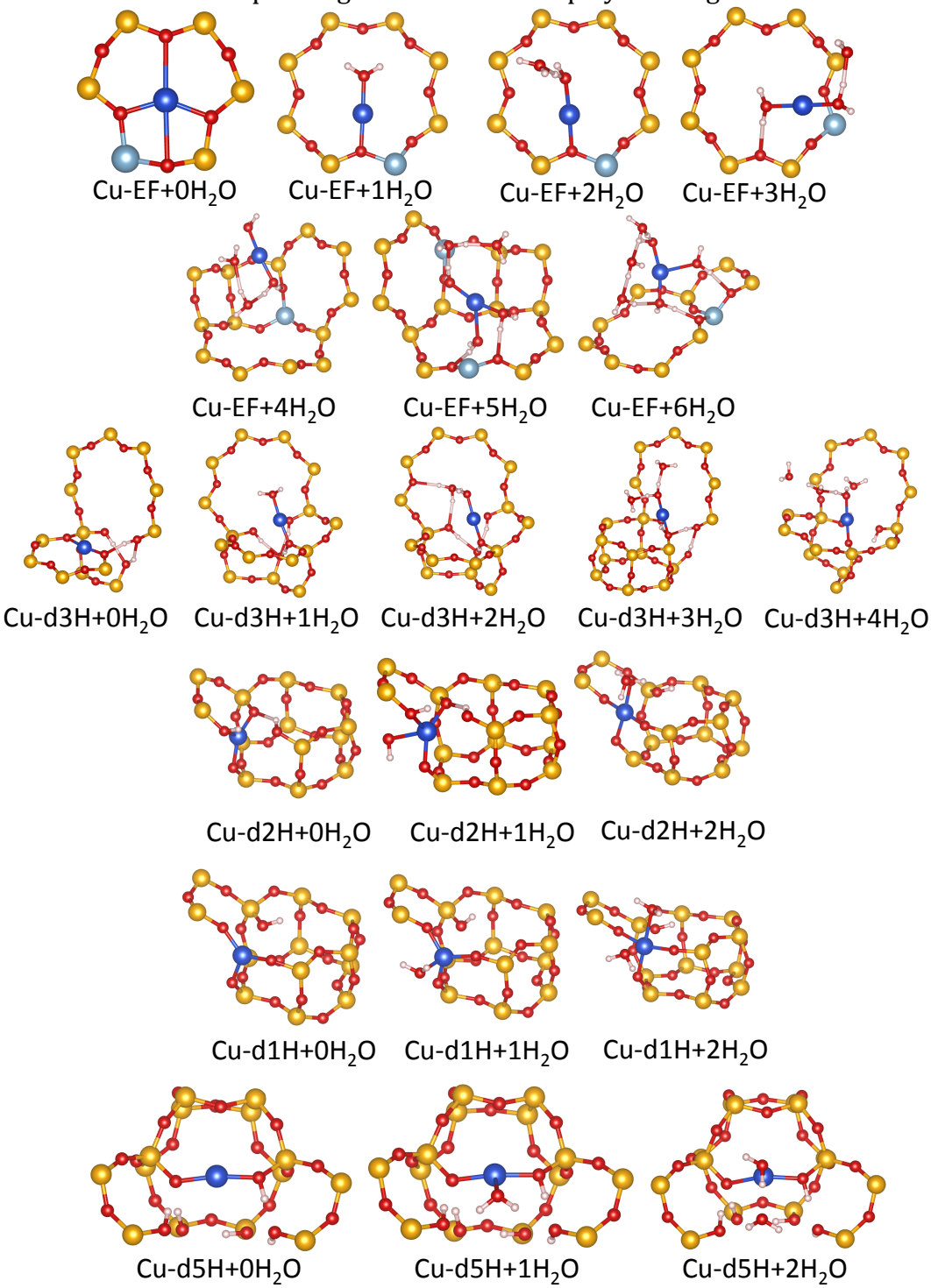

Figure 2: *In the calculated phase diagrams we study extra-framework sites with up to six adsorbed H_2O molecules, silanol defects saturated with three, two or one H atom and one Cu atom with up to four H_2O molecules adsorbed as well as double Si-defects with up to two H_2O adsorbed. Extra-framework sites are labeled by the number of adsorbed water molecules (Cu-EF+mH_2O). Defect sites are labeled following the number of H atoms as Cu-d3H (1 Si removed,*

3H), Cu-d2H (1 Si removed, 2H), Cu-d1H (1 Si removed, 1H) and Cu-d5H (2Si and one O removed, 5H). In atomic representations Si is shown as yellow, O as red, Al atoms as grey-blue, and Cu in blue, respectively.

Next, we focus on the thermodynamics. In the past it has been pointed out that Cu atoms are highly mobile inside the zeolite[11,17]. At a certain coverage of H_2O or NH_3, copper becomes solvated and also the adsorbed molecules show a significant mobility.[18–20,22,24] It has therefore been suggested that static calculations cannot accurately capture the temperature dependence of the thermodynamic potentials, such as the specific heat (c_V) and entropy (S). To address this problem we perform *ab-initio* molecular dynamics calculations as implemented in the Vienna Ab-Initio Simulation Package (VASP) for all structures using the PBE-TS[40,41] functional at 300 K, 400 K, 500 K, 600 K, 700 K and 800 K (for details, see methods section) and calculate the temperature dependent Helmholtz free energy $A(T)$ as[42]

$$A(T) = E(T) + \frac{1}{\beta}\left(\left\langle \exp(\beta \Delta E \right\rangle_T^{eq}\right).$$

Here β stands for $1/k_BT$, and the term in angle brackets denotes the time average for the system equilibrated at temperature T. $E(T)$ is the average potential energy calculated as ensemble average over the DFT potential energies and ΔE stands for the difference between the average potential energy and DFT potential energies calculated at each step along the MD trajectory. In a subsequent step we rewrite $A(T)$ as

$$A(T) = E(0) + (c_v - S)T\,,$$

Here c_V is the heat capacity of the system at constant volume and S is the entropy of the system. We furthermore calculate $U(T)$, the internal energy of the system, as average over kinetic and potential energies and use the relation

$$U(T) = E(0) + c_v T$$

to extract both, c_v and S from $A(T)$ and $U(T)$. Numerical values, plots, and linear fits for all studied sites and reference states are given in SI, Fig. S1, while we focus on Cu-EF, Cu-d3H and Cu-d5H in the subsequent discussion.

A and U show an almost perfect linear dependence ($R^2>0.98$) on temperature for all studied configurations (see SI Fig. S1). At the same time, we find significant differences in the temperature dependence of A and U for sites at the different anchoring points and with the number of adsorbed H_2O molecules, which is reflected in differences for c_v, S and c_v-S. c_v (see Fig. 3 (a)) generally increases with the number of H_2O molecules. However, the increase is not linear and a particularly large increase is found for Cu-d3H when moving from zero to one H_2O molecule and for Cu-EF when moving from two to three H_2O molecules and Cu-d5H in general. Additionally c_v is generally higher for the defect anchored copper, which is not surprising considering the presence of several OH bonds, which show very high vibrational frequencies. Interestingly S shows an almost perfect linear increase with adsorbed water molecules for all sites. Only when moving between one and two adsorbed H_2O molecules for Cu-d5H, deviations from the linear behavior are found (see Fig. 3 (b)). Combining c_v and S now gives the temperature dependence of A (Fig.

3 (c)). Generally we find an increase of c_v–S with the number of water molecules. As the previously discussed values for c_v and S imply, this increase is not monotonous.

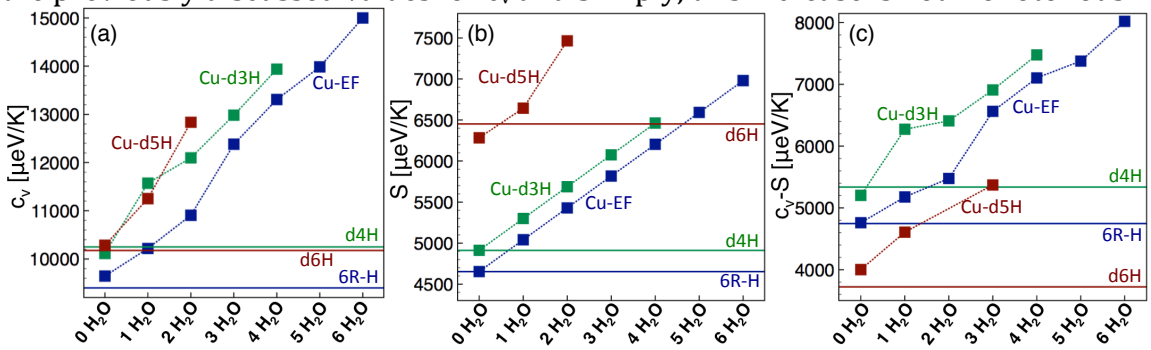

Figure 3: *We calculate the temperature dependent internal energy (U) and Helmholtz free energy (A). Studying the temperature dependence of these quantities allows us to extract the specific heat (c_V; panel a), the entropy (S; panel b) and temperature dependence of A (c_v-S; panel c). These quantities are shown for the Cu extra framework (Cu-EF, blue squares and blue dashed lines), Cu-d3H sites (green squares and green dashed lines) and Cu-d5H (red squares and red dashed lines) with respect to the number of adsorbed H_2O molecules. Furthermore the c_v, S and c_v-S values for the reference states of an H-saturated Al site (EF-H), single defect site (d4H) and double defect site (d6H) are shown as reference. A(T) and U(T) along with values for d2H and d1H sites are shown in Supporting Information Fig. S1.*

So far the discussion was focused on the temperature dependence of U and A, which were calculated using the PBE-TS functional. At the same time it is well known that GGA functionals, such as PBE, are not well suited to accurately describe the interactions between single Cu atoms and molecules.[15] We therefore rely on the Adiabatic Connection Fluctuation Dissipation Theorem in its Random Phase Approximation (RPA),[43] a high level post-DFT method, which has been shown to lead to more reliable energies for similar systems,[44,45] and correct the energies as

$$U^{RPA}(T) = E^{RPA} + U^{PBE}(T) - E^{PBE}.$$

Here U indicates the temperature dependent internal energy, while E indicates values obtained from static calculations for optimized structures. $A^{RPA}(T)$ is obtained as described above.

To compare the relative stability of Cu in its different bonding environments, we focus on μ^{Cu}, the chemical potential of copper, which is calculated as

$$\mu_C^{Cu}(T,P) = A^C(T) - A^{ref}(T) - \frac{2m-k}{2}\mu^{H_2O}(T,P) - \frac{k}{4}\mu^{O_2}(T,P)$$

Here C stands for the given structure, ref for its reference state (*e.g.* the zeolite unit cell containing Al and one proton or a defect), m for the number of adsorbed water molecules, k for the number of removed hydrogen atoms, μ^{H_2O} for the chemical potential of H_2O and μ^{O_2} for the chemical potential of O_2, which we use as reference gases. Additionally we calculate c_v and S for the gas phase molecules O_2 and H_2O as described above, whereby the pressure dependence of the gas phase chemical potentials is introduced by

$$\mu^{M,g}(T,P) = A^M(T) + k_B T \ln(P^{M,g}/P_0),$$

where M, g stands for the molecule M in gas phase, $P^{M,g}$ stands for the partial pressure of molecule M in the gas phase and P_0 is a reference pressure of 1 bar. Since experimental measurements were performed under vacuum, we keep the relative ratios of P^{H_2O} and P^{O_2} constant at e^4, which corresponds to relative partial pressures of O_2 and H_2O in air.

In a subsequent step we use μ^{Cu} and calculate phase diagrams for two scenarios, one where no defects are present and another one where defects as anchoring points for Cu were included. The corresponding results are displayed in Fig. 4. For the case where only extra framework Cu was allowed (Fig. 4 (a)), it can be seen that - as expected - Cu hydrated with six H_2O molecules is most stable at low temperatures and high H_2O partial pressures. However, as soon as temperature is increased and the partial pressure of H_2O becomes lower Cu-EF-2H_2O becomes the most stable structure. Only at high temperatures and low H_2O partial pressures all H_2O desorbs from Cu and Cu-EF-0H_2O is most stable. At low temperatures and high water partial pressures the phase diagram does not change when defects are included (see Fig. 4 (b)). However, at rather elevated temperatures and low H_2O partial pressures, Cu-d5H-0H_2O becomes favorable. These results clearly indicate that at elevated temperatures and low partial H_2O pressures Cu will migrate to framework defects, as long as they are present in the material. At the same time, Cu in the single Cu-d3H, Cu-d2H or Cu-d1H defect positions is never found to be stable.

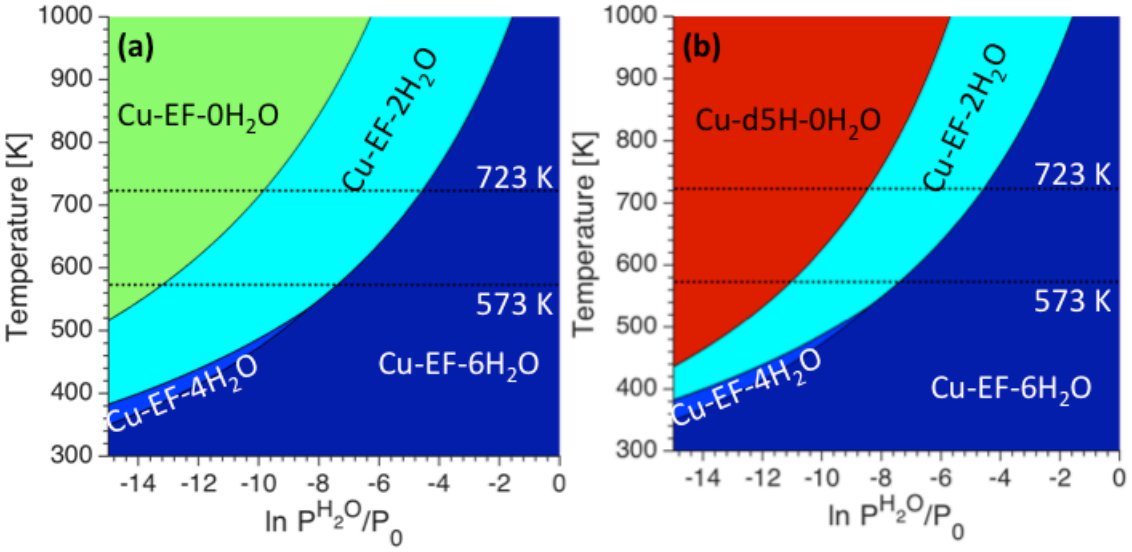

Figure 4: *We used A(T) values to calculate phase diagrams (a) without defects and (b) including defects. The different colors in the phase diagrams correspond to areas in the T/P space of lowest A(T) of the site given in the legend. Dashed lines indicate pretreatment temperatures of 573 K and 723 K.*

Absorption spectra

Experimental measurements:

To allow for comparability between theoretical calculations and experimental measurements, we synthesized two different zeolite samples with Si/Al ratios of 35. The high Si/Al ratio is chosen to obtain isolated Al atoms and minimize the pairing

of Al atoms in the framework. Firstly, we followed the fluorine route (material obtained denoted as SSZ-13-F), which is used to synthesize highly crystalline SSZ-13 with a low concentration of framework defects at high Si/Al ratios[46]. In the second case, we followed the most frequently used synthesis route using NaOH (material obtained denoted as SSZ-13-OH),[47] which is associated with the formation of a larger number of framework defects. The as-synthesized SSZ-13-OH zeolite was washed and treated in ammonia, a process used to exchange Na^+ ions with NH_4^+ ions. Then the zeolite was calcined to desorb NH_3 and generate the protonated form of the material. Subsequently solid-state-ion-exchange was performed for both materials using Cu(I)Cl as Cu(I) precursor to create Cu(I) extra framework species.[29,48,49] Additionally, we treated the material with hydrogen at 773 K for 3h to remove excess Cl. Finally, the materials were treated under vacuum (10^{-2} mbar) at 573 K or 723 K for 24 h. For absorption measurements the samples were transferred to a glove box (< 1ppm H_2O and O_2) and spectra were recorded after 5 minutes. Results for both samples, SSZ-13-F and SSZ-13-OH, are displayed in Fig. 5 (a) and (b), respectively. After pretreatment at 573 K spectra for both samples are very similar and show a main peak centered around 42500 cm^{-1} (blue line Fig. 5). When the samples are pretreated at 723 K, a second peak centered around 30600 cm^{-1} appears, and significant differences between spectra for SSZ-13-F and SSZ-13-OH can be observed. For the SSZ13-OH sample this peak has an intensity of about 1/3-1/4 of the main peak. For the SSZ-13-F sample, on the other hand, this peak only appears as a weak shoulder. At the same time we do not observe any significant spectroscopic features in the 5000 cm^{-1}-20000 cm^{-1} range, which have been associated with the presence of Cu(II) or Cu dimers in the past[35,50]. We therefore conclude that these sites are at best a minority species in the present material. We furthermore exclude the presence of Cu^0, which has not been observed for temperature programmed reduction of Cu-SSZ13 with H_2 up to 873 K[51].

Additionally we were interested in the impact of the glove box atmosphere at room temperature on the samples. We therefore studied the time evolution of the spectra after pretreatment at 723 K and measured absorption spectra for both samples after 1 h, 24 h and 13 days in a glove box atmosphere, which are displayed in Fig. S2 (a) and (b), respectively. We observe that the low energy peak stays constant in relative intensity for about one day, after two weeks it either completely disappears (SSZ13-F) or loses about half of its intensity (SSZ13-OH). At the same time, weak features in the 5000 cm^{-1}-20000 cm^{-1} range appear over time which have been associated with the formation of Cu(II)-OH or Cu dimers[35,50].

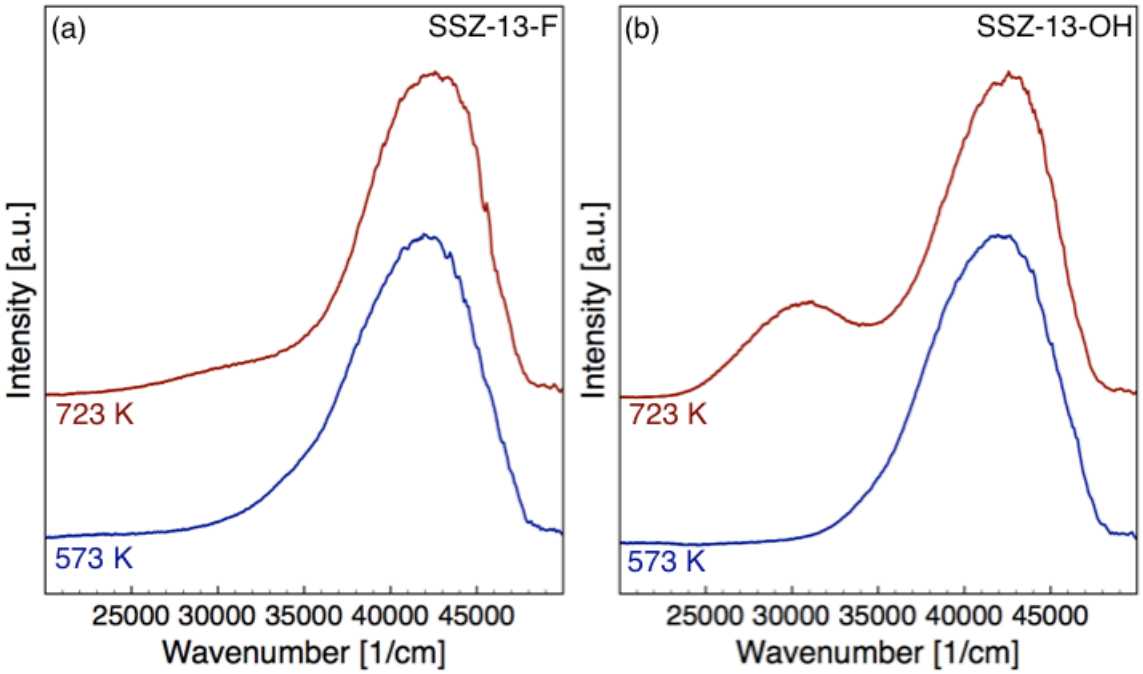

Figure 5: *Absorption spectra for two SSZ-13 materials at Si/Al=35 synthesized (a) using the fluoride route (SSZ-13-F) and (b) conventional synthesis using NaOH (SSZ-13-OH). Spectra collected after exposure to the glove-box atmosphere for 5 minutes after vacuum treatment at 573 K (blue line) and 723 K (red line) are displayed.*

Calculated spectra and assignment of experimental features:

The observed experimental absorption spectra between the two materials differ significantly; we rely on our theoretical calculations to make relevant assignments. Due to the computational cost associated with the calculation of optical spectra, we focus our analysis on four different sites, which were predicted to be most stable at low partial H_2O pressures in the phase diagrams discussed above (Cu-EF-0H_2O, Cu-EF-2H_2O, Cu-d5H-0H_2O and Cu-d5H-1H_2O). As a first step we focused on the fully periodic structures optimized using PBE-TS and calculated optical excitation energies within a time dependent Hartree-Fock like linear response scheme.[52] In our approach the ground state orbitals were determined using hybrid Hartree-Fock density functional theory calculations (TD-HSE) and the electron-hole interactions were approximated by a screened Coulomb kernel using a mixing parameter α=0.4 (TD-HSE). This α value agrees well with literature values for [$CuCl_4$][53]. More details motivating this choice are given in the theoretical methods section. We performed three different calculations for each structure, one using spin-orbit coupling (SOC)[54] to identify all possible, optically active transitions, one calculation without enabling singlet-triplet transitions and one calculation enabling singlet-triplet transitions. The results for all structures are shown in Fig. S3. In Fig. S3 the spectra without singlet-triplet transitions show excellent agreement with the spectra calculated using SOC. However, for almost all structures, the weak intensity centered between 30000 cm^{-1} and 35000 cm^{-1} found in SOC calculations is not correctly described in calculations without including SOC corrections and singlet-triplet transitions. Thus, we included singlet-triplet transitions into the calculations as a next step. This is

possible by removing the Hartree part of the electron-hole Hamiltonian (*i.e.*, the bubble diagrams), when calculating the excitation energy using the TD-HSE scheme. Calculations explicitly including singlet-triplet transitions correctly predict this specific transition. Combining these pieces of information reveals that the observed spectra correspond to the five 3d 4s singlet-singlet transitions, which are optically forbidden for perfect symmetry, but become optically active due to the distortion of the ligand field and one singlet-triplet transition.

However, these static calculations correspond to a system at 0 K, whereas, as shown above, at finite temperature, Cu changes its coordination regularly. To take this effect into account, we use the trajectory obtained from *ab-initio* molecular dynamics simulations at 300 K. For the obtained structures the optical absorption spectrum was calculated as an average of the spectra of a set of structural snapshots[55]. We performed convergence tests with the number of structural snapshots and we again perform calculations including and not including singlet-triplet transitions for each structure. We found reasonably well-converged spectra for 300 structures (the convergence tests are shown in the supporting information Fig. S4), and the obtained spectra are displayed in Fig. S5 of SI. Static and dynamic spectra show similar features (see SI, Fig. S3), but significant broadening with the main maxima red-shifted by about 1000 cm^{-1} is observed, if dynamics are taken into account.

We focus our analysis on the structures most prevalent in the phase diagrams of Fig. 4. The calculated spectra for the Cu-EF+2H_2O, Cu-d5H+1H_2O sites at finite temperature are shown in Fig. 6. As shown above, for all three spectra a singlet-triplet and a triplet-triplet transition are optically active. We choose the simplest approach and focus on two different transitions, i.e. the singlet-singlet transition for Cu-EF+2H_2O and singlet-triplet transitions of Cu-d5H+1H_2O to reconstruct the spectra (the exact weights are given in the figure caption of Fig. 6) and indeed excellent agreement is found between the experimentally observed spectra five minutes after vacuum treatment at 573 K (Fig. 6 (a) and 723 K (Fig. 6 (b)). A closer analysis reveals that the main peak at ~42500 cm^{-1} results from a singlet-singlet d-s transition for the 8R+2H_2O structure. The side peak, however, directly results from the singlet-triplet transitions at Cu-d5H+1H_2O. The modeled spectra show excellent qualitative and quantitative agreement with errors of 70 cm^{-1} for the main peak and and 480 cm^{-1} for the side peak in spectra after pretreatment at 723 K.

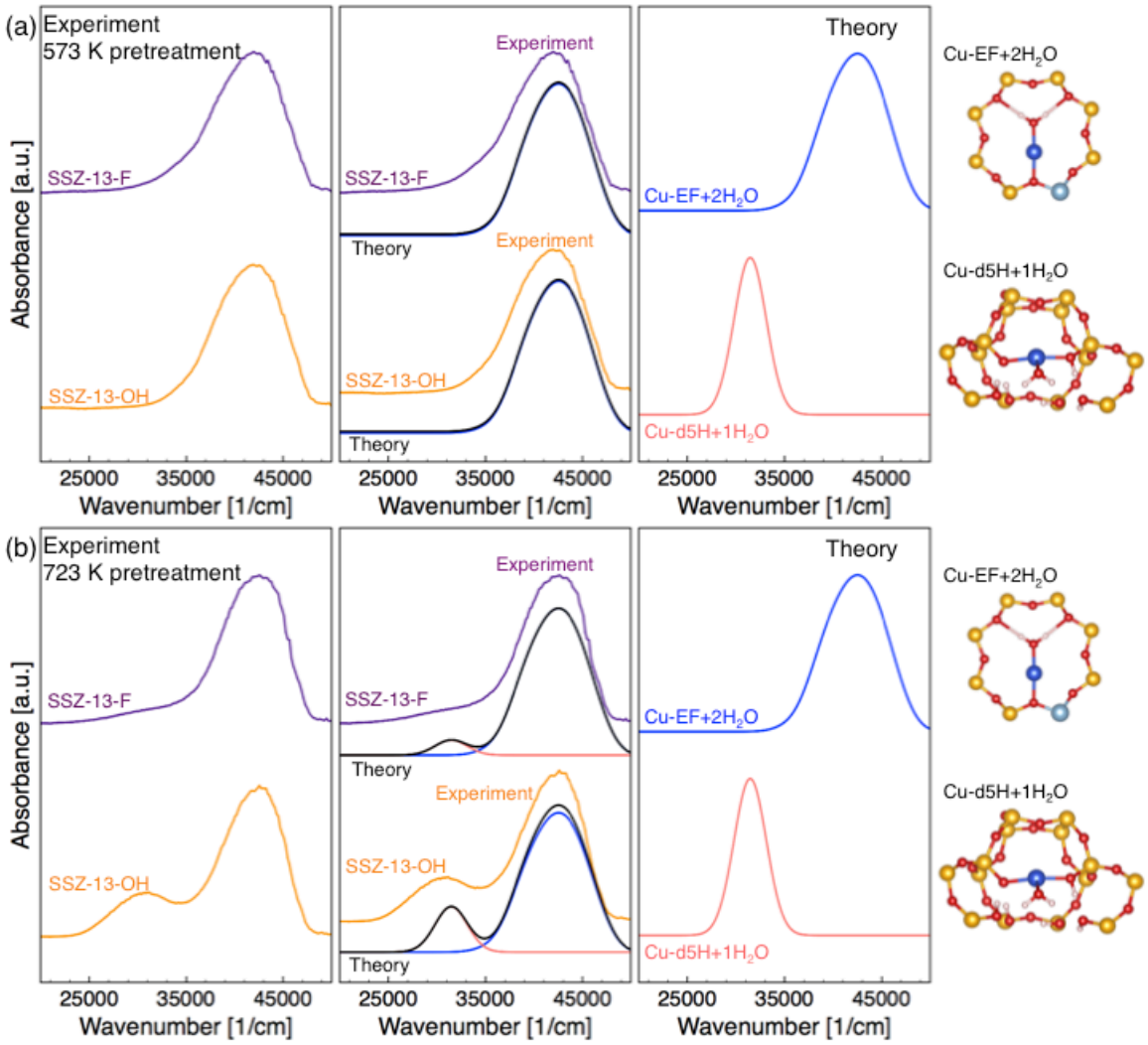

Figure 1: *A comparison between experimentally measured absorption spectra after pretreatment at (a) 573 K and (b) 723 K and 5 minutes exposure to glove-box atmosphere (left lt panels) and theoretical spectra for the Cu-EF+2H_2O, and Cu-d5H+1H2O (right panels). In the middle panels experimental and theoretical spectra are compared. Theoretical spectra are (a) spectra for the singlet-singlet transition for Cu-EF-2H_2O or (b) spectra for obtained by mixing 1.6%/98.4% of spectral signals of Cu-d5H+1H2O-t/Cu-EF+2H2O-s, where s denotes singlet-singlet transitions and t denotes singlet-triplet transitions, for SSZ-13-F and 4.6%/95.6% for SSZ-13-OH. A detailed decomposition of the theoretical spectra is shown in supporting information Fig. S4. Light/dark colors in the theoretical spectra correspond to singlet-triplet/singlet-singlet transitions. The color code in the atomistic pictures in the far right corresponds to Fig. 1 and Fig. 2.*

Florian Go
Deleted:

An alternative explanation for the presence of an additional peak in SSZ-13-OH would be the existence of Cu sites in proximity to two Al atoms (Cu^{I}-2Al), a configuration related to the amount of Na cations during synthesis. To exclude this possibility we model the UV-vis spectrum for this site (a detailed discussion is given in the SI, section S4) and find that UV-vis spectra for Cu^{I}-2Al cannot rationalize the observed peaks at 30600 cm^{-1} and 42500 cm^{-1}. Therefore, this type of site will, at

best, only represent a minority of the total distribution of Cu^{I} atoms. At the same time we want to emphasize that the assignments are not unique: a more detailed discussion for alternative assignments is given in the Supporting Information section S5 and an alternative assignment is given in Fig. S7.

Photoluminescence:

Experimental results:

After photoabsorption, the Cu cation is in an excited state, which decays over time and emits light, which can then be measured as emission spectrum. We performed these measurements for our two differently synthesized materials after pretreatment at 723 K and found different peak positions and shapes, as displayed on the left hand side of Fig. 7. For SSZ-13-OH a sharp peak is located at 18350 cm^{-1}, while the peak for SSZ-13-F was significantly wider with a maximum at 20410 cm^{-1}. Both peaks are significantly red-shifted compared to the absorption features; similar spectra have been observed in other zeolite materials[31]. Typically they have been assigned to Cu cations in different extra framework positions, but in the following we will also investigate the impact of defect-anchored Cu on the observed spectra.

Theoretical calculations:

To elucidate the differences between the two materials, we relied on modeling. After excitation, the Cu(I) cation is in a $3d^9 4s^1$ configuration and typical lifetimes of the excited state are on the order of 10 μs.[31] Due to this long lifetime, photoluminescence has been suggested to originate from a triplet-singlet transition[32]. We therefore performed molecular dynamics simulations on the triplet potential energy surface to create the structural snapshots. The simulations were again done using the PBE-TS functional restricting the spin to 2 μ_B.

In a first step, we studied the impact of optical excitation on the coordination environment of the cations. Upon excitation the 4s state is occupied, which increases the size of the Cu cation. In this scenario, it is reasonable to assume that the bonding between water and the Cu atom is weakened. The structures in molecular dynamics simulations oscillate around the triplet-structures already predicted in the literature, where the Cu-cation moves out of the six-ring and shows a twofold coordination to the framework.[34,36] When water is adsorbed, Cu is more stable in the eight ring. The basic coordination is similar to the situation in the six ring, but now water binds out of plane to it and is rather mobile.

To arrive at a luminescence spectrum, we furthermore assume reversibility of transitions, *i.e.*, that the photoemission energy for a given structure is equivalent to the excitation energy from the closed shell singlet to the triplet state. In a similar manner to the absorption spectra we again confirmed the presence of singlet-triplet transitions using SOC in static calculations on the triplet potential energy surface and confirmed agreement for explicit inclusion of singlet-triplet transitions in TD-

HSE simulations within 200 cm^{-1}. Consequently, we calculated absorption spectra using the time dependent Hartree-Fock approach for the triplet structures including singlet-triplet transitions and used the lowest transition as emission spectrum. To calculate the spectra we used 300 snapshots along the molecular dynamics trajectory of the triplet structures.

We focus on the luminescence spectra for the Cu-EF site with no and one adsorbed water molecule and the Cu-d5H site with one adsorbed H_2O molecule to reconstruct the luminescence spectra of the two studied materials (see Fig. 7). While the spectrum of SSZ-13-OH is almost exclusively composed of the defect emission signal, SSZ-13-F is mainly composed of the signal at the extra framework site (75% without water, 25% with water) and only a minority signal (~7%) is required to reproduce the basic shape of the observed spectrum. The modeled spectra show excellent agreement with the experimental measurements with errors smaller than 400 cm^{-1}. Similar to absorption, spectra are not unique and an alternative assignment is given in Supporting Information, section S5.

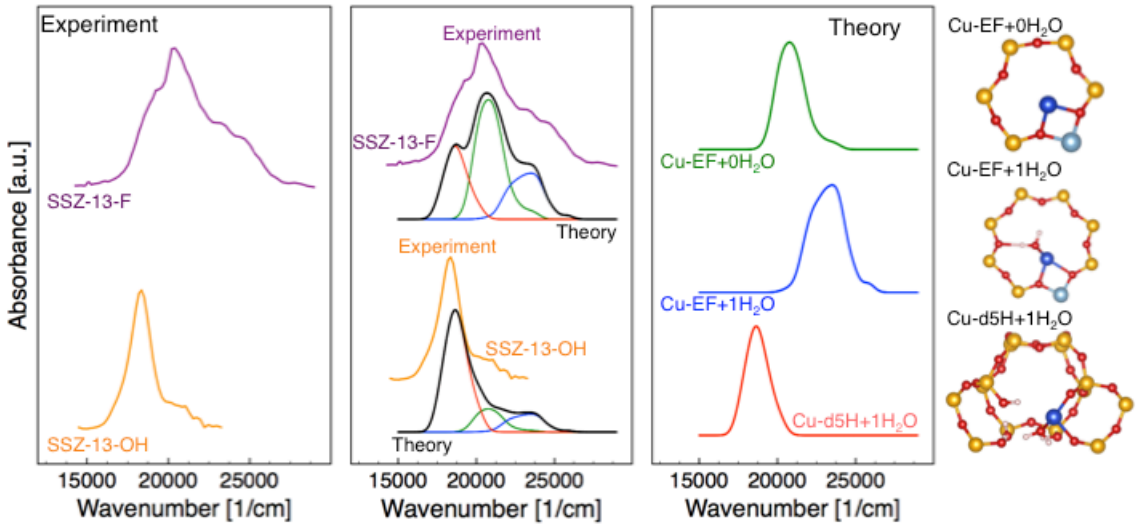

Figure 7: *Photoluminescence spectra for Cu-sites in SSZ-13. On the left hand side the experimental spectra for the two studied zeolites SSZ-13-OH and SSZ-13-F are given. On the right hand side the different theoretical spectra are displayed and in the middle the comparison between a superposition of theoretical spectra as well as the experimental results are given. The color code in the atomistic pictures corresponds to that of Fig. 1 and Fig. 2.*

Discussion:

The results presented here show that it is possible to qualitatively and quantitatively predict accurate optical absorption and photoluminescence spectra of Cu^{I}-sites in zeolites. Importantly, the absorption spectra agree with theoretically calculated phase diagrams for SSZ-13. To achieve the excellent agreement between measured spectra and phase diagrams, we explicitly calculated temperature dependent free energies using *ab-initio* molecular dynamics calculations. These calculations reveal that very different temperature corrections are found for the adsorption of subsequent water molecules. We indeed find that entropy increases

linearly with the addition of water molecules, which agrees with previous reports in the literature.[18,26] However, entropic corrections are slightly larger than the entropy of a single water molecule and the increase in the specific heat is non-linear. The explicit calculation of temperature dependence for all the sites leads to phase diagrams, which predict the migration of Cu to framework defects at high temperature and low partial H_2O pressures (see Fig. 4 (b)). This finding is corroborated by measured and calculated UV-vis spectra after pretreatment at 573 K and 723 K. While after pretreatment at 573K no defect-anchored Cu is present (Fig. 6 (a)), significant amounts of Cu in defect sites are found after pretreatment at 723 K (Fig. 6 (b)). Comparing this transition to the phase diagrams in Fig. 4, such a transition would happen for partial H_2O pressures between e^{-9} bar and e^{-11} bar, which agrees well with experimentally applied partial H_2O pressures of $e^{-11.5}$ bar.

As pointed out in the main text the assignments made in UV-vis and luminescence spectra are not unique, i.e. different assignments are possible. However, we clearly identify that the main peak in measured UV-vis spectra results from a singlet-singlet charge transfer transition of EF Cu^I sites. At the same time our calculations indicate that only a singlet-triplet transition at a defect site, where a covalent bond between O and Cu is formed, will lead to the side-peak at ~30600 cm^{-1} observed after high temperature pretreatment and we make the assignments based on the calculated phase diagrams. However, Cu^I bound to larger defects or grain boundaries, which were not included in the phase diagrams, might also show similar signals and cannot be excluded at this moment in time. Spectral decomposition indicates that only a small fraction of the signal in UV-vis measurements stems from defect anchored Cu (4.6 and 1.6 %, for SSZ-13-OH and SSZ-13-F, respectively). However, this assignment neglects that singlet-triplet transitions are expected to be less intense and a far larger portion of Cu could be located at defects. Additionally we find the occupation of the defect site to be rather stable over an extended period of time. We therefore expect significant diffusion barriers for the migration from extra framework sites to defects and vice-versa.

It is furthermore interesting to see that monovalent Cu in defect sites is stabilized at higher temperatures and low partial H_2O pressures. This observation is particularly important for the selective catalytic reduction of NO_x using NH_3 ($deNO_x$-SCR), the main industrial application of Cu exchanged SSZ-13. Here, it is expected that during aging extended framework defects are generated[56–58] and a significant loss in activity is observed[59]. At high temperatures, as e.g. encountered in the regeneration cycle of the catalyst, the monovalent Cu might migrate to the defects, where it is expected to show different catalytic properties. Different catalytic activity might be caused by the changes in electronic structure (as seen by the changes in the observed spectra) or by the loss of Cu coordination to water or NH_3 at the defect sites. The migration of Cu to defects and the formation of covalent Cu-O bonds might be connected to the observation of CuO_x species, which have been reported to build up after high temperature aging[60]. However, further work will be necessary to study the interactions of defect anchored Cu and NH_3 and the impact of this type of site on $deNO_x$-SCR.

While phase diagrams predict the correct adsorption spectra, *i.e.*, a larger fraction of defect-anchored Cu in SSZ-13-OH compared to SSZ-13-F, the excellent agreement is lost for luminescence spectra. In particular luminescence spectra for SSZ-13-OH are almost exclusively composed by defect-anchored Cu, despite only a minority defect spectrum in absorption. We explain this mismatch with the formation of excitons in the zeolite matrix. These excitons will be trapped at the energetically favored Cu defect sites, where they recombine. This interpretation agrees well with the long lifetimes of the excited states (on the order of 10 μs).[31] The almost exclusive recombination of excitons at the defect sites has two very specific implications. First, the luminescence spectra at defects are red-shifted with respect to the luminescence at extra-framework sites. Second, the emission peaks are narrower and a significant increase in intensity is found for emission at the defect site. Recently, transition metal exchanged zeolites have been reported to be excellent photo-emitters[8,9]. We expect that the introduction of framework defects can be used to specifically tailor the light-color and frequency range as well as the intensity of the observed emissions. At the same time, the selective recombination of excitons and holes at specific sites could be used in photocatalytic applications.

Conclusions:

In this contribution we studied the coordination of monovalent Cu^{I}-cations in zeolite SSZ-13 using phase diagrams and correlated them to optical absorption and luminescence spectra. By combining *ab-initio* molecular dynamics simulations and post-DFT simulations we calculated accurate temperature dependent free energies and found that at high temperatures and low partial H_2O pressures Cu migrates from extra-framework positions to defect sites. Using a combination of molecular dynamics simulations and time dependent Hartree-Fock calculations, we confirmed this phenomenon by optical absorption spectroscopy, which allows the assignment of features in experimentally recorded absorption spectra to defect-anchored Cu. Interestingly, the intensity of the defect signal is significantly magnified in luminescence spectra of Cu-SSZ-13. We interpret this occurrence as the generation of excitons in the zeolite lattice, which preferentially recombine at the defect sites.

The results presented here have profound implications on deNO_x-SCR catalysis in aged catalysts, where a significant amount of framework defects is present and Cu might migrate to them under reaction conditions. Furthermore, insights into optical spectroscopy reveal a strategy to modify the luminescence spectrum of the material. It will be interesting to see how these insights can be used to further optimize materials for specific applications.

Methods:

Theoretical setup: All calculations were carried out using the Vienna Ab-Initio Simulation Package (VASP).[38,39] It is a plane wave code, where the electron-ion

interactions are described within the Projector Augmented Wave method.[61,62] In all calculations an energy cut-off of 420 eV was applied. Due to the single site nature of the copper-sites and the comparatively large unit cell a k-point sampling restricted to the Γ-point was appropriate for all Brillouin zone integrations. In all structure optimizations, DFT in the generalized gradient approximation in the parameterization of Perdew, Burke and Ernzerhof[40] was applied. Dispersion corrections were added using the method suggested by Tkatchenko and Scheffler.[41] For static calculations a force convergence criterion of 0.01 eV/Å was applied. The ideal proton distribution and Cu anchoring was identified as minimum structure of all possible proton positions at 0 K. Excited state structures were optimized by enforcing the triplet spin state. In molecular dynamics simulations an Anderson-thermostat with a collision probability of 0.015 for each atom and a time step of 1 fs was used to keep the system at 300 K. As mentioned in the main text, optical spectra were calculated every 100 fs for 300 images (total sampling time 30 ps). For optical calculations the number of occupied and empty bands in the calculations was increased to 3040. In a first step, the wave functions were optimized using a HSE-type functional with the exact exchange increased to 40%. To determine the optical properties, the time dependent Casida equation[52] was solved with the amount of exact exchange taken into account by the mixing parameter α, where the amount of exact exchange is fixed to α and the density functional theory exchange set to 1-α. α was parameterized for static calculations of the 6R emission peak and experimental measurements, as outlined in the supporting information section S5. The chosen value of α=0.4 is close to what one would expect for weakly screening materials such as zeolites and is also close to the values optimized for $CuCl_4$, where an optimized α =0.385 leads to smallest deviations between theoretically calculated and experimentally measured spectra[53]. We want to emphasize that α was parameterized for only one specific transition, whereas the excellent agreement with all the remaining transitions justifies this choice. Absorption spectra were obtained by applying a Gaussian broadening of 2000 cm^{-1} to the lowest five optical transitions. To obtain luminescence spectra, the reversibility of optical transitions was assumed and they were calculated as the lowest transition of the absorption spectrum at the excited state geometries; a Gaussian broadening of 500 cm^{-1} was applied. The differences in broadening are used to take the different resolutions of the used instruments in the given energy ranges into account. The unit cell chosen in this work is described in the literature[36]. However, to take the expansion of the system, due to the presence of one Al atom, into account we increased the volume to 830 $Å^3$.

Experimental Setup:

Zeolite Synthesis: SSZ-13 zeolites with a Si/Al ratio of 35 were prepared from both hydroxide and fluoride media (SSZ-13-OH and SSZ-13-F). Zeolite SSZ-13-OH was synthesized following a procedure described elsewhere.[47] For the preparation of the synthesis gel NaOH (0.19 g, ≥97%, Sigma-Aldrich) was dissolved in deionized water (23.5 g) followed by the addition of the structure directing agent TMAda-OH (3.89 g, 25%, SACHEM ZeoGen 2825). After dissolving aluminum hydroxide (0.12 g, 50-5% Al_2O_3, Sigma-Aldrich), fumed silica powder (2.75 g, 0.007 μm average particle size,

Sigma-Aldrich) was added under vigorous stirring until a homogeneous gel was observed. The gel with a molar composition of 10 SDA : 10 NaOH : 1.43 Al_2O_3 : 100 SiO_2 : 2200 H_2O was then transferred into a 45 mL Teflon-lined stainless steel autoclave, before hydrothermal crystallization was carried out at 160° C in a rotating oven at 60 rpm. After the synthesis the solid was recovered by filtration and washed with deionized water and acetone. Finally the zeolite powder was dried in a convection oven at 110° C and calcined at 650° C for 6h with a ramp of 3° C/min under an air flow. To transform the Na form of the SSZ-13 (Na-SSZ-13-OH) into its protonic form (H-SSZ-13-OH) the zeolite was ion-exchanged in 3 cycles with a 1 M ammonium nitrate solution at 80° C for 12h. After each cycle the zeolite was filtered, washed with water and dried at 110° C over night. After the final exchange the sample was subjected to an additional calcination step at 580° C for 6h under an air flow. The Si/Al ratio of 35 was confirmed by ICP-AES.

SSZ-13-F was prepared by adapting the method reported by Eilertsen *et al.*[46]. Al powder (0.05 g, 99.99%, Acros) was dissolved in TMAda-OH solution (26.6 g, 25%, SACHEM, ZeoHen 2825). After complete dissolution a mixture of Ethanol (8 g, 200 Proof) and tetraethyl-orthosilicate (13 g, TEOS, 98%, Sigma-Aldrich) was added dropwise. After hydrolysis of the TEOS the synthesis gel was heated up to 50° C under stirring to evaporate excess of water. The resulting mixture was ground prior to the dropwise addition of hydrofluoric acid (1.28 g, 48 wt%, Sigma-Aldrich). Homogeneity was ensured by mixing with a PTFE spatula. The final synthesis gel with the composition 50 SDA:50 HF:1.43 Al_2O_3:100 SiO_2:300 H_2O was then charged into a Teflon-lined stainless steel autoclave and hydrothermal crystallization was carried out at 155° C for 7 days in a rotating oven (60 rpm). The crystalline product was collected by filtration and washed with deionized water and acetone before drying it at 110° C. To remove the SDA the material was calcined at 600° C for 6h under an air flow. The Si/Al ratio of 35 was confirmed by ICP-AES. The crystal structure of both materials was confirmed using Powder X-Ray Diffraction (see Fig. S9 in the Supporting Information).

Cu Ion exchange and UV-vis: The zeolite was dried in a He flow at 500° C (3 h, 5 K/min) prior to the solid-state-ion exchange (SSIE)[29,49] The ion exchange was performed by grinding the appropriate amount of $Cu^{I}Cl$ with the required amount of zeolite inside of a glovebox (<1 ppm H_2O and O_2) for 15 min. The sample was treated in a He flow at 600° C (4 days, 2° C/min) and reduced in a 4% H_2/N_2 flow at 500° C (3h, 2 K/min). ICP analyses indicate Cu/Al ratios of 0.34 (SSZ-13-OH) and 0.30 (SSZ-13-F) and a Na/Al ratio of 0.03 (SSZ-13-OH) and 0.008 (SSZ-13-F). After reduction, the samples were exposed to air and re-reduced at 450° C in a 4% H_2/N_2 flow for 3h. Immediately after the samples were treated at 300° C or 450° C under 10^{-2} mbar vacuum for 24h, the samples were transferred to a glovebox and UV/Vis analyses were performed thereafter with a Maya2000 Pro UV/Vis Spectrophotometer (Ocean Optics), equipped with a deuterium/halogen light source (DH-200-BAL from Mikropack) using $BaSO_4$ as matrix, in diffuse reflectance mode. Again crystalinity of SSZ-13-OH after ion exchange and high temperature vacuum treatment was confirmed using Powder X-Ray Diffraction (see Fig. S10 in the Supporting Information).

Photoluminescence: To allow measurements in an inert atmosphere, samples were placed between two high purity fused quartz coverslips (Ted Pella, Inc.), which were than sealed in the glove box using Torr Seal vacuum epoxy. Steady-state photoluminescence spectra were collected using an ISS K2 spectrometer, with a 300 Watt xenon arc lamp source and an excitation wavelength of 250 nm. Sample normal was positioned 34° from incident excitation wavelength. Emission spectra were collected from 230-700 nm, with 5 nm increments and a monochromator with 8 nm/mm reciprocal linear dispersion. A Newport FSQ-WG320 long-pass filter was used in the emission path to filter scattering of the excitation beam. In these measurements the quartz slides showed a significant signal in the investigated energy range. To correct for it and signals of the zeolite after calcination, we measured a blank sample containing only the as prepared H-SSZ-13 samples. To obtain the emission spectrum, the H-SSZ-13-OH spectrum was normalized with respect to the intensity of the main peak and subtracted from the Cu-SSZ-13 spectrum.

Supporting Information: The Supporting Information is available free of charge via the Internet at http:/pubs.acs.org. The Supporting Information includes information about the temperature dependence of A and U, the time evolution of the UV-vis spectra in a low pressure system, calculated absorption spectra and their convergence, absorption spectra of the Cu^{I}-2Al site, alternate assignments for observed optical transitions, the parameterization of the exact exchange parameter in optical calculations and XRD spectra for materials after synthesis as well as SSZ-13-OH after ion exchange and high temperature vacuum treatment.

Acknowledgements: F. Göltl, S. Conrad and J. Wheeler acknowledge discussion with J. Dědeček (J. Heyrovský Institute of Physical Chemistry, Prague). The authors acknowledge financial support from the University of Wisconsin-Madison and the Wisconsin Alumni Research Foundation (WARF). F. Göltl and M. Mavrikakis acknowledge support from the National Science Foundation, grant number CHE-1800284. S. Conrad acknowledges funding from grant ETH-38 12-1 and P. Wolf acknowledges funding from SNF grant No. 200021_146661. F.Göltl, M. Mavrikakis. and I. Hermans acknowledge computational time at Phoenix Supercomputer, which is supported in part by National Science Foundation Grant CHE-0840494 and National Energy Research Scientific Computing Center (NERSC), a DOE Office of Science User Facility supported by the Office of Science of the U.S. Department of Energy under Project Nos. m2070-Zeo-genome and mp-351. This research was in part performed using the compute resources and assistance of the UW-Madison Center For High Throughput Computing (CHTC) in the Department of Computer Sciences. The CHTC is supported by UW-Madison, the Advanced Computing Initiative, the Wisconsin Alumni Research Foundation, the Wisconsin Institutes for Discovery, and the National Science Foundation, and is an active member of the Open Science Grid, which is supported by the National Science Foundation and the U.S. Department of Energy's Office of Science. F. Göltl acknowledges computational time at the Extreme Science and Engineering Discovery Environment (XSEDE), which is supported by National Science Foundation grant number ACI-1548562.

References:

(1) Bull, I.; Xue, W. M.; Burk, P.; Boorse, R. S.; Jaglowski, W. M.; Kroemer, G. S.; Moini, A.; Patchett, J. A.; Dettling, J. C.; Caudle, M. T. Copper CHA Zeolite Catalysts. US Patent 7 601 662 B2, 2009.

(2) Beale, A. M.; Gao, F.; Lezcano-Gonzalez, I.; Peden, C. H. F.; Szanyi, J. Recent Advances in Automotive Catalysis for NO_x Emission Control by Small-Pore Microporous Materials. *Chem. Soc. Rev.* **2015**, *44*, 7371–7405.

(3) Paolucci, C.; Di Iorio, J. R.; Ribeiro, F. .; Gounder, R.; Schneider, W. F. Catalysis Science of NOx Selective Catalytic Reduction with Ammonia over Cu-SSZ-13 and Cu-SAPO-34. In *Advances in Catalysis*; Elsevier Inc., 2016; Vol. 59, pp 1–107.

(4) Ravi, M.; Ranocchiari, M.; van Bokhoven, J. A. The Direct Catalytic Oxidation of Methane to Methanol—A Critical Assessment. *Angew. Chemie - Int. Ed.* **2017**, *56* (52), 16464–16483.

(5) Dinh, K. T.; Sullivan, M. M.; Serna, P.; Meyer, R. J.; Dincă, M.; Román-Leshkov, Y. Viewpoint on the Partial Oxidation of Methane to Methanol Using Cu- and Fe-Exchanged Zeolites. *ACS Catal.* **2018**, *8* (9), 8306–8313.

(6) Mlinar, A. N.; Baur, G. B.; Bong, G. G.; Getsoian, A.; Bell, A. T. Propene Oligomerization over Ni-Exchanged Na-X Zeolites. *J. Catal.* **2012**, *296*, 156–164.

(7) Mlinar, A. N.; Shylesh, S.; Ho, O. C.; Bell, A. T. Propene Oligomerization Using Alkali Metal- and Nickel-Exchanged Mesoporous Aluminosilicate Catalysts. *ACS Catal.* **2014**, *4* (1), 337–343.

(8) Fenwick, O.; Coutiño-Gonzalez, E.; Grandjean, D.; Baekelant, W.; Richard, F.; Bonacchi, S.; De Vos, D.; Lievens, P.; Roeffaers, M.; Hofkens, J.; et al. Tuning the Energetics and Tailoring the Optical Properties of Silver Clusters Confined in Zeolites. *Nat. Mater.* **2016**, *15* (June), 1–11.

(9) Grandjean, D.; Coutiño-Gonzalez, E.; Cuong, N. T.; Fron, E.; Baekelant, W.; Aghakhani, S.; Schlexer, P.; D'acapito, F.; Banerjee, D.; Roeffaers, M. B. J.; et al. Origin of the Bright Photoluminescence of Few-Atom Silver Clusters Confined in LTA Zeolites. *Science (80-.).* **2018**, *361* (6403), 686–690.

(10) Göltl, F.; Bulo, R. E.; Hafner, J.; Sautet, P. What Makes Copper-Exchanged SSZ-13 Zeolite Efficient at Cleaning Car Exhaust Gases? *J. Phys. Chem. Lett.* **2013**, *4*, 2244–2249.

(11) Göltl, F.; Sautet, P.; Hermans, I. The Impact of Finite Temperature on the Coordination of Cu Cations in the Zeolite SSZ-13. *Catal. Today* **2016**, *267*, 41–46.

(12) Göltl, F.; Müller, P.; Uchupalanun, P.; Sautet, P.; Hermans, I. Developing a Descriptor-Based Approach for CO and NO Adsorption Strength to Transition Metal Sites in Zeolites. *Chem. Mater.* **2017**, *29*, 6434–6444.

(13) Godiksen, A.; Stappen, F. N.; Vennestrøm, P. N. R.; Giordanino, F.; Rasmussen, S. B.; Lundegaard, L. F.; Mossin, S. Coordination Environment of Copper Sites in Cu-CHA Zeolite Investigated by Electron Paramagnetic Resonance. *J. Phys. Chem. C* **2014**, *118* (40), 23126–23138.

(14) Borfecchia, E.; Beato, P.; Svelle, S.; Olsbye, U.; Lamberti, C.; Bordiga, S. Cu-CHA-a Model System for Applied Selective Redox Catalysis. *Chem. Soc. Rev.* **2018**, *47* (22), 8097–8133.

(15) Göltl, F.; Hafner, J. Structure and Properties of Metal-Exchanged Zeolites Studied Using Gradient-Corrected and Hybrid Functionals. III. Energetics and Virational Spectroscopy of Adsorbates. *J. Chem. Phys.* **2012**, *136* (6), 064503.

(16) McEwen, J. S.; Anggara, T.; Schneider, W. F.; Kispersky, V. F.; Miller, J. T.; Delgass, W.

N.; Ribeiro, F. H. Integrated Operando X-Ray Absorption and DFT Characterization of Cu-SSZ-13 Exchange Sites during the Selective Catalytic Reduction of NO x with NH 3. *Catal. Today* **2012**, *184* (1), 129–144.

(17) Göltl, F.; Sautet, P.; Hermans, I. Can Dynamics Be Responsible for the Complex Multipeak Infrared Spectra of NO Adsorbed to Copper(II) Sites in Zeolites? *Angew. Chemie - Int. Ed.* **2015**, *54* (27), 7799–7804.

(18) Paolucci, C.; Parekh, A. A.; Khurana, I.; Di Iorio, J. R.; Li, H.; Albarracin Caballero, J. D.; Shih, A. J.; Anggara, T.; Delgass, W. N.; Miller, J. T.; et al. Catalysis in a Cage: Condition-Dependent Speciation and Dynamics of Exchanged Cu Cations in Ssz-13 Zeolites. *J. Am. Chem. Soc.* **2016**, *138* (18), 6028–6048.

(19) Göltl, F.; Love, A. M.; Hermans, I. Developing a Thermodynamic Model for the Interactions Between Water and Cu in the Zeolite SSZ-13. *J. Phys. Chem. C* **2017**, *121*, 6160–6169.

(20) Lomachenko, K. A.; Borfecchia, E.; Negri, C.; Berlier, G.; Lamberti, C.; Beato, P.; Falsig, H.; Bordiga, S. The Cu-CHA $DeNO_x$ Catalyst in Action: Temperature-Dependent NH_3-Assisted Selective Catalytic Reduction Monitored by Operando XAS and XES. *J. Am. Chem. Soc.* **2016**, *138*, 12025–12028.

(21) Moreno-González, M.; Hueso, B.; Boronat, M.; Blasco, T.; Corma, A. Ammonia-Containing Species Formed in Cu-Chabazite as per in Situ EPR, Solid-State NMR, and DFT Calculations. *J. Phys. Chem. Lett.* **2015**, *6* (6), 1011–1017.

(22) Petitjean, H.; Chizallet, C.; Berthomieu, D. Modeling Ammonia and Water Co-Adsorption in Cu^{I}-SSZ-13 Zeolite Using DFT Calculations. *Ind. Eng. Chem. Res.* **2018**, *57* (47), 15982–15990.

(23) Marberger, A.; Petrov, A. W.; Steiger, P.; Elsener, M.; Kröcher, O.; Nachtegaal, M.; Ferri, D. Time-Resolved Copper Speciation during Selective Catalytic Reduction of NO on Cu-SSZ-13. *Nat. Catal.* **2018**, *1* (3), 221–227.

(24) Paolucci, C.; Khurana, I.; Parekh, A. A.; Li, S.; Shih, A. J.; Li, H.; Iorio, J. R. Di; Albarracin-caballero, J. D.; Yezerets, A.; Miller, J. T.; et al. Dynamic Multinuclear Sites Formed by Mobilized Copper Ions in NO x Selective Catalytic Reduction. *Science (80-.).* **2017**, *5630*, 1–11.

(25) Kwak, J. H.; Varga, T.; Peden, C. H. F.; Gao, F.; Hanson, J. C.; Szanyi, J. Following the Movement of Cu Ions in a SSZ-13 Zeolite during Dehydration, Reduction and Adsorption: A Combined in Situ TP-XRD, XANES/DRIFTS Study. *J. Catal.* **2014**, *314*, 83–93.

(26) Li, H.; Paolucci, C.; Schneider, W. F. Zeolite Adsorption Free Energies from Ab Initio Potentials of Mean Force. *J. Chem. Theory Comput.* **2018**, *14* (2), 929–938.

(27) Texter, J.; Strome, D. H.; Herman, R. G.; Klier, K. Chemical and Spectroscopic Properties of Cu Containting Zeolites. *J. Phys. Chem.* **1977**, *81* (4), 333–338.

(28) Strome, D. H.; Klier, K. Effects of Carbon Monoxide Absorption on the Luminescence of Reduced Copper-Exchanged Y Zeolite. *J. Phys. Chem.* **1980**, *84* (9), 981–984.

(29) Lamberti, C.; Bordiga, S.; Salvalaggio, M.; Spoto, G.; Zecchina, A.; Giuria, I.-V. P.; Chimica, I.; Torino, P.; Chimica, D.; Uni, V.; et al. XAFS , IR , and UV - Vis Study of the Cu I Environment in Cu I -ZSM-5. *J. Phys. Chem. B* **1997**, *101* (96), 344–360.

(30) Dedecek, J.; Sobalik, Z.; Tvaruzkova, Z.; Kaucky, D.; Wichterlova, B. Coordination of Cu Ions in High-Silica Zeolite Matrices - Cu^{+} Photoluminescence, Ir of No Adsorbed on Cu^{2+}, and Cu^{2+} Esr Study. *J. Phys. Chem.* **1995**, *99*, 16327–16337.

(31) Dědeček, J.; Wichterlová, B.; Kubát, P. Siting of the Cu^{+} Ions in Dehydrated Ion Exchanged Synthetic and Natural Chabasites: A Cu^{+} Photoluminescence Study. *Microporous Mesoporous Mater.* **1999**, *32*, 63–74.

(32) Nachtigall, P.; Nachtigallova, D.; Sauer, J. Coordination Change of Cu+ Sites in ZSM-5

on Excitation in the Triplet State: Understanding of the Photoluminescence Spectra. *J. Phys. Chem. B* **2000**, *104*, 1738–1745.
(33) Delabie, a; Pierloot, K.; Groothaert, M. H.; Schoonheydt, R. a; Vanquickenborne, L. G. The Coordination of Cu-II in Zeolites - Structure and Spectroscopic Properties. *Eur. J. Inorg. Chem.* **2002**, 515–530.
(34) Göltl, F.; Hafner, J. Structure and Properties of Metal-Exchanged Zeolites Studied Using Gradient-Corrected and Hybrid Functionals. I. Structure and Energetics. *J. Chem. Phys.* **2012**, *136* (6), 064501.
(35) Li, H.; Paolucci, C.; Khurana, I.; Wilcox, L. N.; Göltl, F.; Albarracin-Caballero, J. D.; Shih, A. J.; Ribeiro, F. H.; Gounder, R.; Schneider, W. F. Chemical Science Consequences of Exchange-Site Heterogeneity and Dynamics on the UV-Visible Spectrum Of. *Chem. Sci.* **2019**, *10*, 2373–2384.
(36) Göltl, F.; Hafner, J. Structure and Properties of Metal-Exchanged Zeolites Studied Using Gradient-Corrected and Hybrid Functionals. II. Electronic Structure and Photoluminescence Spectra. *J. Chem. Phys.* **2012**, *136* (6), 064502.
(37) Göltl, F.; Love, A. M.; Schuenzel, S. C.; Wolf, P.; Mavrikakis, M.; Hermans, I. Computational Description of Key Spectroscopic Features of Zeolite SSZ-13 †. *Phys. Chem. Chem. Phys.* **2019**, *21*, 19065–19075.
(38) Kresse, G.; Hafner, J. Ab Initio Molecular Dynamics for Open-Shell Transition Metals. *Phys. Rev. B* **1993**, *48* (17), 13115–13118.
(39) Kresse, G.; Furthmüller, J. Efficiency of Ab-Initio Total Energy Calculations for Metals and Semiconductors Using a Plane-Wave Basis Set. *Comput. Mater. Sci.* **1996**, *6* (1), 15–50.
(40) Perdew, J. P.; Burke, K.; Ernzerhof, M. Generalized Gradient Approximation Made Simple. *Phys. Rev. Lett.* **1996**, *77* (18), 3865–3868.
(41) Tkatchenko, A.; Scheffler, M. Accurate Molecular van Der Waals Interactions from Ground-State Electron Density and Free-Atom Reference Data. *Phys. Rev. Lett.* **2009**, *102* (7), 073005.
(42) Pohorille, A.; Jarzynski, C.; Chipot, C. Good Practices in Free-Energy Calculations. *J. Phys. Chem. B* **2010**, *114*, 10235–10253.
(43) Harl, J.; Kresse, G. Cohesive Energy Curves for Noble Gas Solids Calculated by Adiabatic Connection Fluctuation-Dissipation Theory. *Phys. Rev. B - Condens. Matter Mater. Phys.* **2008**, *77* (4), 1–8.
(44) Göltl, F.; Grüneis, A.; Bučko, T.; Hafner, J. Van Der Waals Interactions between Hydrocarbon Molecules and Zeolites: Periodic Calculations at Different Levels of Theory, from Density Functional Theory to the Random Phase Approximation and Moller-Plesset Perturbation Theory. *J. Chem. Phys.* **2012**, *137* (11), 114111.
(45) Göltl, F.; Michel, C.; Andrikopoulos, P. C.; Love, A. M.; Hafner, J.; Hermans, I.; Sautet, P. Computationally Exploring Confinement Effects in the Methane-to-Methanol Conversion Over Iron-Oxo Centers in Zeolites. *ACS Catal.* **2016**, *6*, 8404–8409.
(46) Eilertsen, E. A.; Arstad, B.; Svelle, S.; Lillerud, K. P.; Al, S. Microporous and Mesoporous Materials Single Parameter Synthesis of High Silica CHA Zeolites from Fluoride Media. *Microporous Mesoporous Mater.* **2012**, *153*, 94–99.
(47) Deka, U.; Juhin, A.; Eilertsen, E. a; Emerich, H.; Green, M. a; Korhonen, S. T.; Weckhuysen, B. M.; Beale, A. M. Confirmation of Isolated Cu^{2+} Ions in SSZ-13 Zeolite as Active Sites in NH_3-Selective Catalytic Reduction. *J. Phys. Chem. C* **2012**, *116* (7), 4809–4818.
(48) Spoto, G.; Zecchina, A.; Bordiga, S.; Ricchiardi, G.; Martra, G.; Leofanti, G.; Petrini, G. Cu(I)-ZSM-5 Zeolites Prepared by Reaction of H-ZSM-5 with Gaseous CuCl: Spectroscopic Characterization and Reactivity towards Carbon Monoxide and Nitric

Oxide. *Appl. Catal. B, Environ.* **1994**, *3* (2–3), 151–172.
(49) Zhang, Y.; Drake, I. J.; Bell, A. T. Characterization of Cu-ZSM-5 Prepared by Solid-State Ion Exchange of H-ZSM-5 with CuCl. *Chem. Mater.* **2006**, *18* (9), 2347–2356.
(50) Ipek, B.; Wulfers, M. J.; Kim, H.; Göltl, F.; Hermans, I.; Smith, J. P.; Booksh, K. S.; Brown, C. M.; Lobo, R. F. Formation of $[Cu_2O_2]^{2+}$ and $[Cu_2O]^{2+}$ toward C-H Bond Activation in Cu-SSZ-13 and Cu-SSZ-39. *ACS Catal.* **2017**, *7* (7), 4291–4303.
(51) Hun Kwak, J.; Zhu, H.; Lee, J. H.; Peden, C. H. F.; Szanyi, J. Two Different Cationic Positions in Cu-SSZ-13? *Chem. Commun. (Camb).* **2012**, *48* (39), 4758–4760.
(52) Casida, M. E. Generalization of the Optimized-Effective-Potential Model to Include Electron Correlation: A Variational Derivation of the Sham-Schlüter Equation for the Exact Exchange-Correlation Potential. *Phys. Rev. A* **1995**, *51* (3), 2005–2013.
(53) Szilagyi, R. K.; Metz, M.; Solomon, E. I. Spectroscopic Calibration of Modern Density Functional Methods Using $[CuCl4]^{2-}$. *J. Phys. Chem. A* **2002**, *106* (12), 2994–3007.
(54) Steiner, S.; Khmelevskyi, S.; Marsmann, M.; Kresse, G. Calculation of the Magnetic Anisotropy with Projected-Augmented-Wave Methodology and the Case Study of Disordered $Fe_{1-x}Co_x$ Alloys. *Physcial Rev. B* **2016**, *93*, 224425.
(55) Hemelsoet, K.; Qian, Q.; De Meyer, T.; De Wispelaere, K.; De Sterck, B.; Weckhuysen, B. M.; Waroquier, M.; Van Speybroeck, V. Identification of Intermediates in Zeolite-Catalyzed Reactions by in Situ UV/Vis Microspectroscopy and a Complementary Set of Molecular Simulations. *Chem. - A Eur. J.* **2013**, *19* (49), 16595–16606.
(56) Schmidt, J. E.; Oord, R.; Guo, W.; Poplawsky, J. D.; Weckhuysen, B. M. Nanoscale Tomography Reveals the Deactivation of Automotive Copper-Exchanged Zeolite Catalysts. *Nat. Commun.* **2017**, *8* (1), 1–8.
(57) Kovarik, L.; Washton, N. M.; Kukkadapu, R.; Devaraj, A.; Wang, A.; Wang, Y.; Szanyi, J.; Peden, C. H. F.; Gao, F. Transformation of Active Sites in Fe/SSZ-13 SCR Catalysts during Hydrothermal Aging : A Spectroscopic, Microscopic, and Kinetics Study. *ACS Catal.* **2017**, *7*, 2458–2470.
(58) Albarracin-Caballero, J. D.; Khurana, I.; Di Iorio, J. R.; Shih, A. J.; Schmidt, J. E.; Dusselier, M.; Davis, M. E.; Yezerets, A.; Miller, J. T.; Ribeiro, F. H.; et al. Structural and Kinetic Changes to Small-Pore Cu-Zeolites after Hydrothermal Aging Treatments and Selective Catalytic Reduction of NO_x with Ammonia. *React. Chem. Eng.* **2017**, *2* (2), 168–179.
(59) Song, J.; Wang, Y.; Walter, E. D.; Washton, N. M.; Mei, D.; Kovarik, L.; Engelhard, M. H.; Prodinger, S.; Wang, Y.; Peden, C. H. F.; et al. Toward Rational Design of Cu / SSZ-13 Selective Catalytic Reduction Catalysts : Implications from Atomic-Level Understanding of Hydrothermal Stability. *ACS Catalyysis* **2017**, *7* (x), 8214–8227.
(60) Gao, F.; Szanyi, J. Applied Catalysis A , General On the Hydrothermal Stability of Cu / SSZ-13 SCR Catalysts. *Appl. Catal. A, Gen.* **2018**, *560* (May), 185–194.
(61) Blöchl, P. E. Projector Augmented-Wave Method. *Phys. Rev. B* **1994**, *50* (24), 17953–17979.
(62) Kresse, G.; Joubert, D. From Ultrasoft Pseudopotentials to the Projector Augmented-Wave Method. *Phys. Rev. B* **1999**, *59* (3), 1758–1775.

Graphical Abstract:

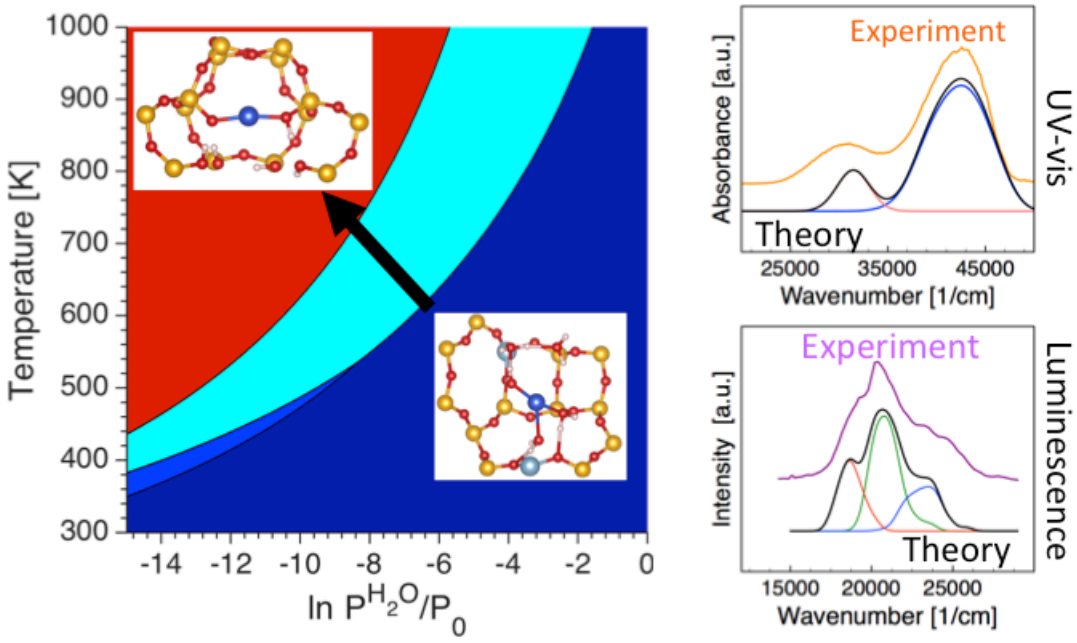

Supporting Information for:

UV-vis and Photoluminescence Spectroscopy to Understand the Coordination of Cu Cations in the Zeolite SSZ-13

Florian Göltl[1,2], Sabrina Conrad[1,3], Patrick Wolf[1,3], Philipp Müller[1], Alyssa M. Love[1], Samuel P. Burt[2], Jamie N. Wheeler[1], Robert J. Hamers[1], Kerstin Hummer[4], Georg Kresse[4], Manos Mavrikakis[2], Ive Hermans[1,2]

[1] University of Wisconsin, Madison, Department of Chemistry, University Avenue 1101, 53706 Madison, Wisconsin, USA
[2] University of Wisconsin - Madison, Department of Chemical and Biological Engineering, 1415 Engineering Drive, 53706 Madison, Wisconsin, USA
[3] Department of Chemistry and Applied Biosciences, ETH Zurich, Vladimir-Prelog-Weg 1-5, 8093 Zurich, Switzerland
[4] University of Vienna, Faculty of Physics, Computational Materials Physics, Sensengasse 8/12, 1090 Vienna, Austria
Corresponding author: fgoeltl@wisc.edu, hermans@chem.wisc.edu

S1: Temperature dependent A and U

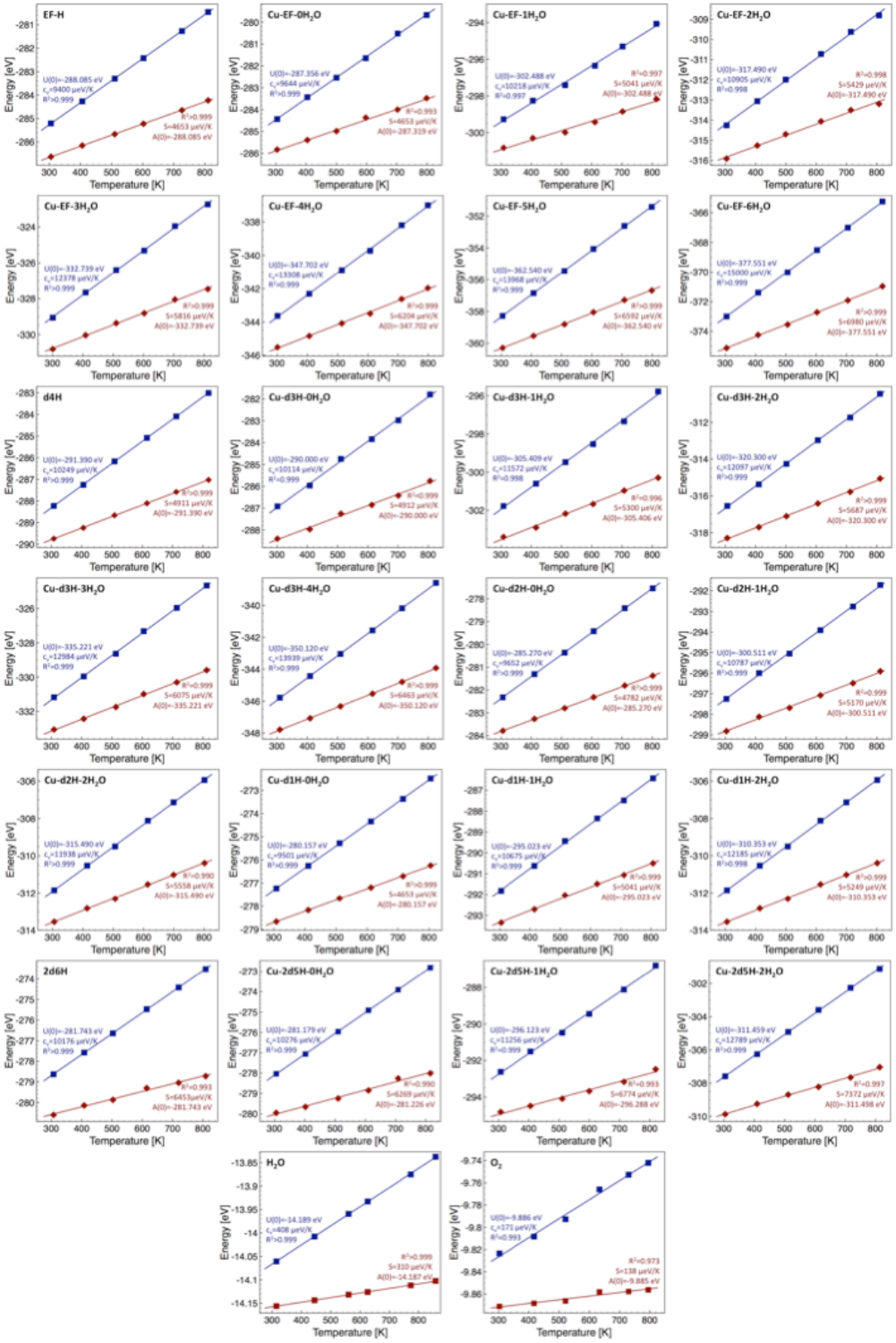

Figure S1*: Temperature dependent Helmoltz free energy A(T) (red) and internal energy U(T) (blue) for the different sites studied in this work. Symbols represent values calculated at the given temperature using molecular dynamics simulations, lines correspond to linear fits. Fitting parameters, specific heat c_v and entropy S are given in the figure legends.*

S2: Time evolution of absorption spectra

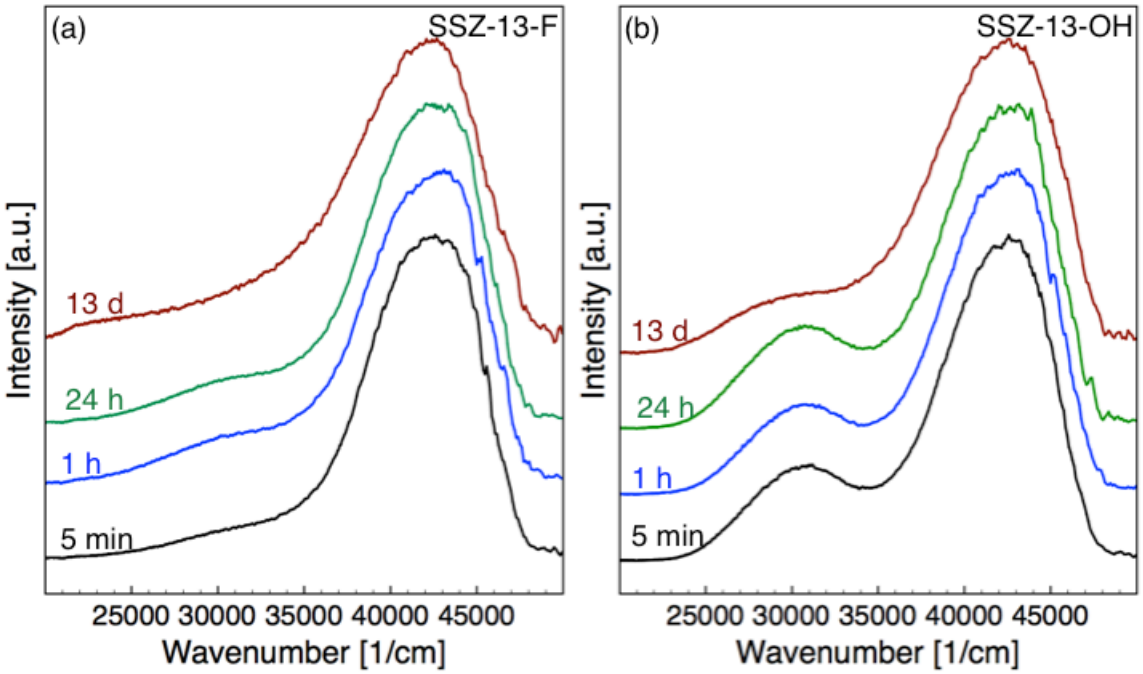

Figure S2: *Absorption spectra for two SSZ-13 materials at Si/Al=35 synthesized (a) using the fluoride route (SSZ-13-F) and (b) conventional synthesis using NaOH (SSZ-13-OH). Spectra collected after exposure to the glove-box atmosphere for 5 minutes (black line), 1 hour (blue line), 24 hours (green line) and 13 days (red line) are displayed.*

S3: Theoretically calculated absorption spectra

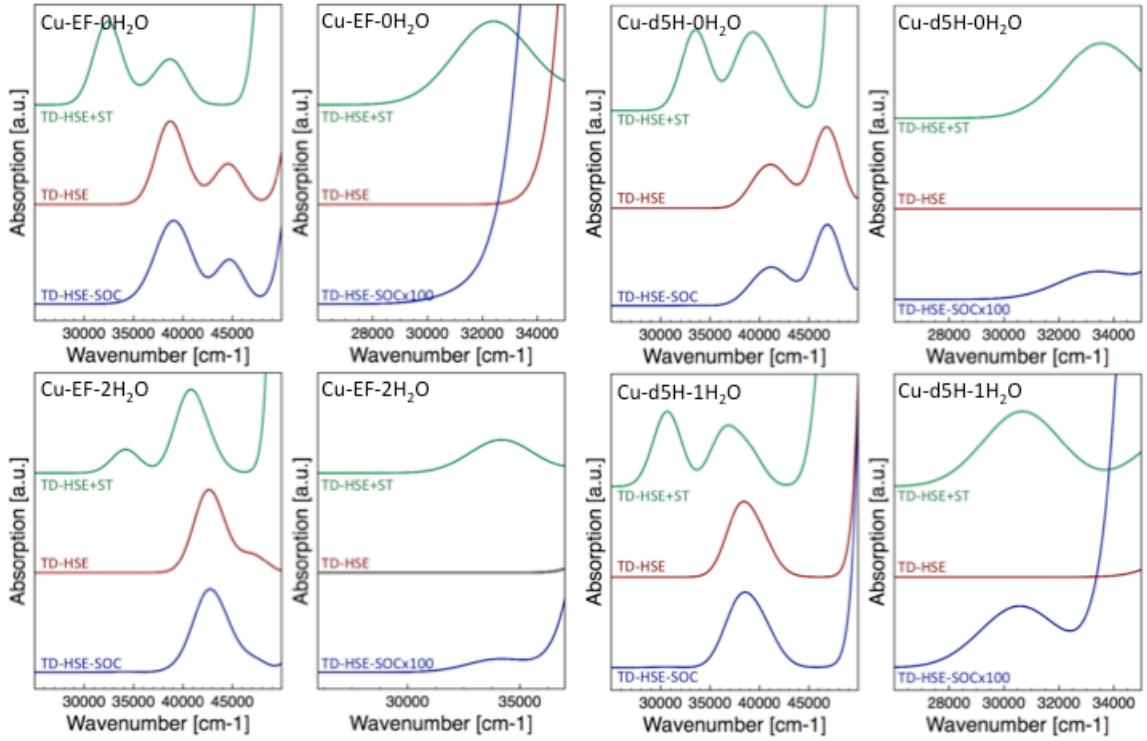

Figure S3: *Absorption spectra for the different sites calculated using spin-orbit coupling (TD-HSE-SOC, blue lines), only singlet-singlet transitions (TD-HSE, red lines) and singlet-triplet transitions (TD-HSE+ST, green lines). It can be seen that the lowest transition in TD-HSE-SOC calculations is well reproduced by TD-HSE-ST, while the other transitions are well described using TD-HSE.*

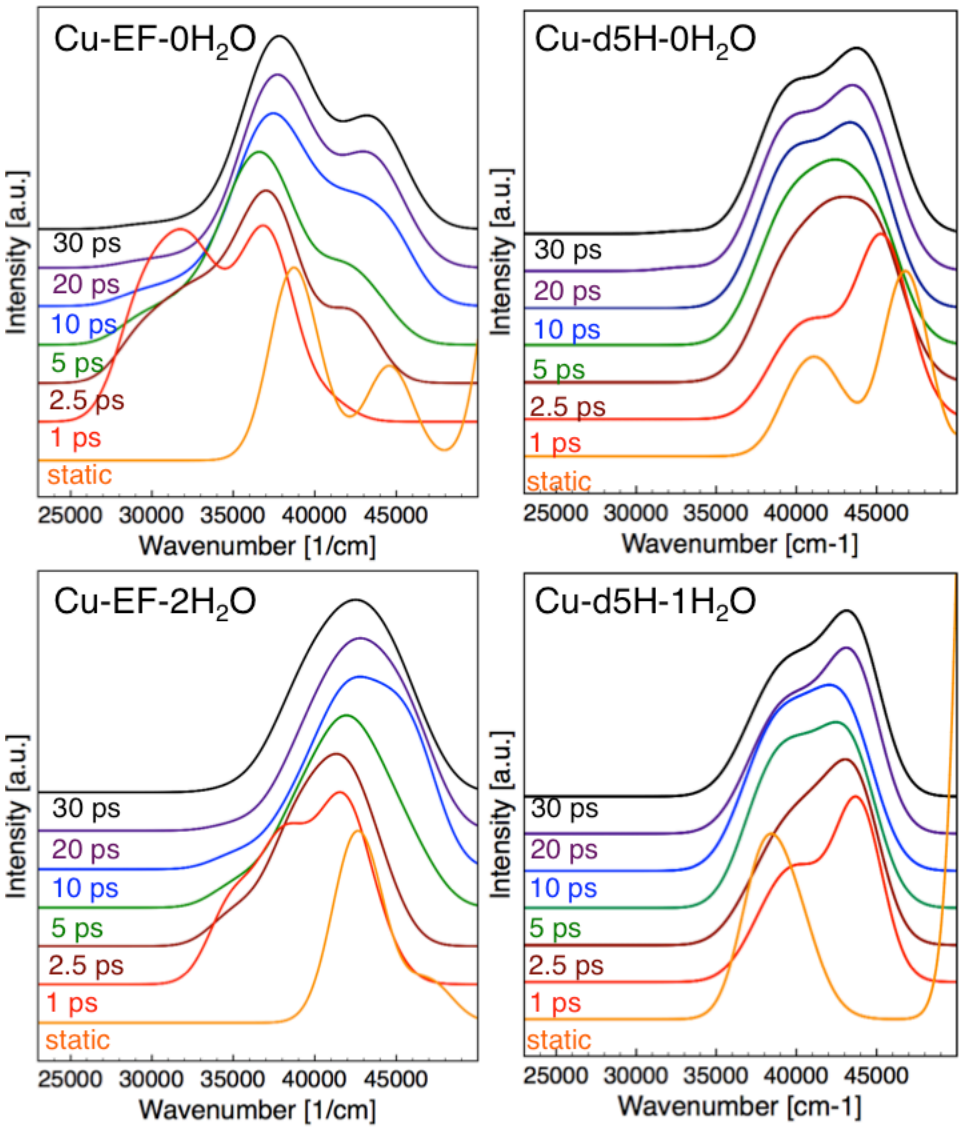

Figure S4: *Evolution of TD-HSE spectra with sampling times for the sites studied in this work. Orange lines show statically calculated spectra, red lines spectra after 1 ps, dark red lines spectra after 2.5 ps, green lines spectra after 5 ps, blue lines spectra after 10 ps, purple lines spectra after 20 ps and black lines spectra after 30 ps. Spectra are calculated as superposition of spectra taken for snapshots every 100 fs. Minimal changes between spectra after 20 ps and 30 ps indicate conversion after these timescales.*

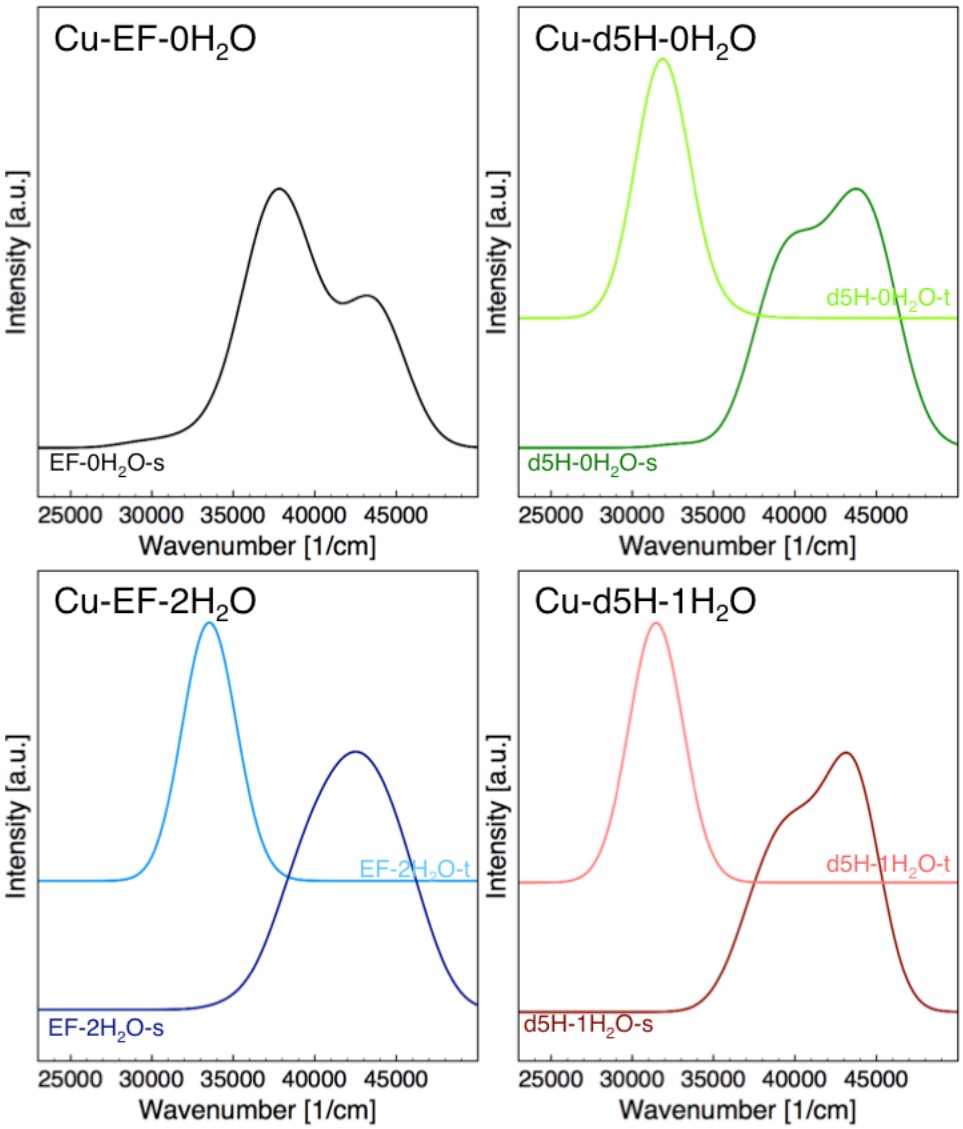

Figure S5*: Finite temperature spectra calculated for absorption at the different sites. Dark colored lines show singlet-singlet transitions, light colored lines show singlet-triplet transitions.*

S4: UV-vis spectra of the Cu^{I} 2Al site

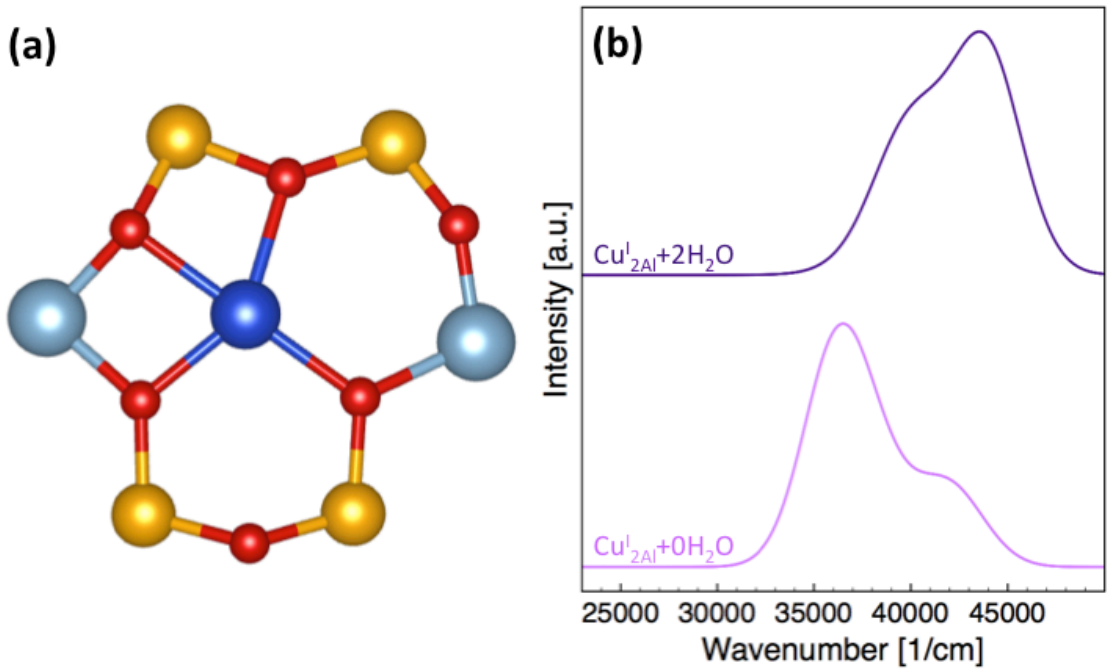

Figure S6*: To exclude a significant contribution of a Cu site placed in a 6R containing 2 Al atoms, we modeled UV-vis spectra for the site shown in (a). A Cu^{I} site was generated by adding an H atom in the O(4) position close to one Al atom. (b) Dynamic absorption spectra for Cu^{I} bonded in a 6R close to 2Al atoms with no and two H_2O molecules adsorbed. The lavender line shows the spectrum without adsorbed H_2O atoms and the purple line shows the site with two adsorbed H_2O atoms. Both spectra do not agree with the experimentally observed spectra shown in Figure 5 B. We therefore assume that this site is only a minority of the total Cu distribution in the material.*

S5: Alternate Assignments of spectroscopic features

As discussed in the main text, alternate assignments of UV-vis and luminescence features displayed in Fig. 5, 6, and 7 are possible. To do so we calculate spectra for d3H anchored Cu and the corresponding results are shown in Fig. S7 and Fig. S8, respectively. We find that it is possible to reproduce UV-vis spectra after pretreatment at 723 K by using a complex mixture of signals from EF+ $2H_2O$, d3H+0H2O and d3H+1H2O (see Fig. S7 and the weights given in the figure caption). Similarly the low energy luminescence peak can be reproduced as luminescence for the d3H+0H2O site. While it is possible to reproduce these two spectra with either of the Cu(I) sites anchored in defects, EF Cu does not show signals in the given range.

Based on this information we conclude that it is not possible to unambiguously assign a signal to one specific defect site, but only to defect anchored Cu. Potentially

also Cu(I) anchored in larger silanol defects or grain boundaries in the zeolite will show similar spectroscopic features.

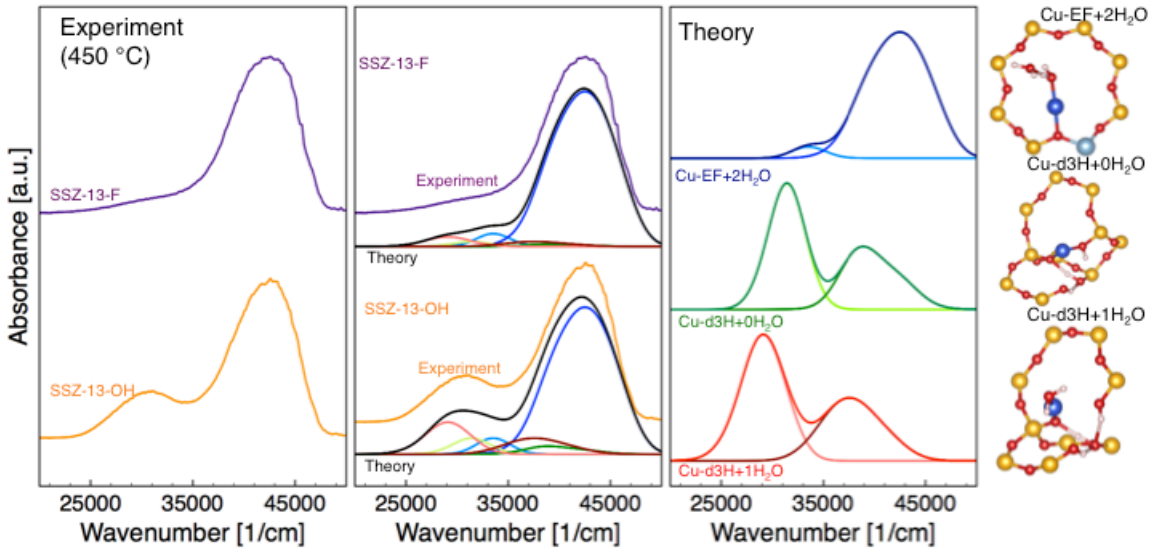

Figure S7: *A comparison between experimentally measured absorption spectra after pretreatment at 723 K and 5 minutes exposure to glove-box atmosphere (left panel) and theoretical spectra for the Cu-EF+2H₂O, Cu-d3H+0H₂O and Cu-d3H+1H₂O (right panel). In the middle panel experimental and theoretical spectra are compared. Theoretical spectra are obtained by mixing 0.4%/0.3%/1.3%/0.9%/5.6%/91.5% of spectral signals of Cu-d3H+0H2O-t/Cu-d3H+0H2O-s/Cu-d3H+1H2O-t/Cu-d3H+1H2O-s/Cu-EF+2H2O-t/Cu-EF+2H2O-s, where s denotes singlet-singlet transitions and t denotes singlet-triplet transitions, for SSZ-13-F and 1.4%/1.0%/4.0%/2.8%/6.4%/84.4% for SSZ-13-OH. Light/dark colors in the theoretical spectra correspond to singlet-triplet/singlet-singlet transitions. The color code in the atomistic pictures in the far right corresponds to Fig. 1 and Fig. 2.*

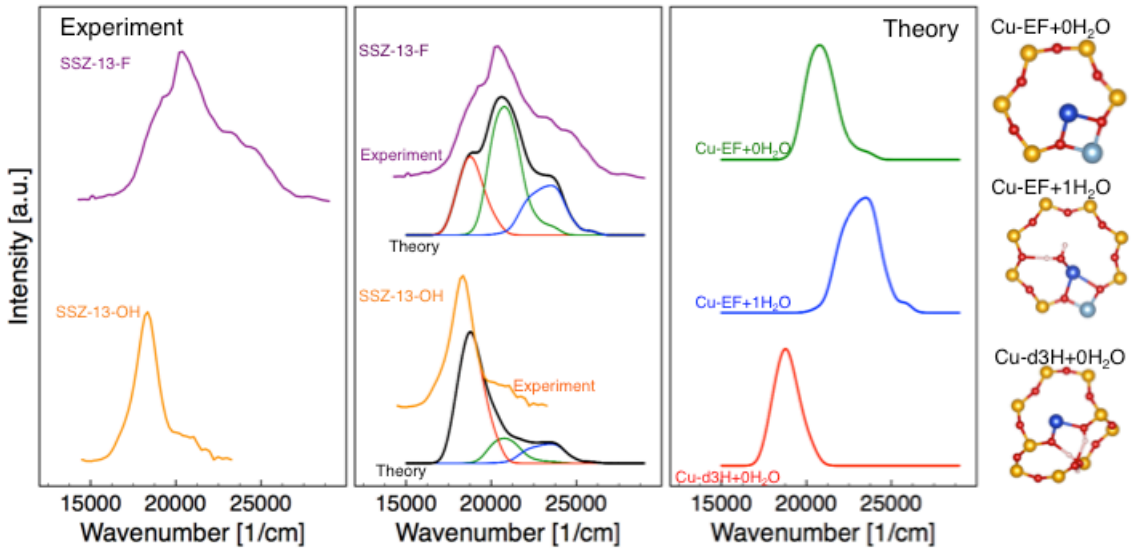

Figure S8: *Photoluminescence spectra for Cu-sites in SSZ-13 using spectra for Cu-EF-0H₂O,Cu-EF-1H₂O and Cu-d3H+0H₂O. On the left hand side the experimental spectra for the two studied zeolites SSZ-13-OH and SSZ-13-F are given. On the right hand side the different theoretical*

spectra are displayed and in the middle the comparison between a superposition of theoretical spectra as well as the experimental results are given. The color code in the atomistic pictures corresponds to that of Fig. 1 and Fig. 2 in the main text.

S6: Emission signal vs. exact exchange parameter

***Table S3**: Position of the emission signal for Cu in the six-ring in dependence on the choice of the exact exchange parameter α. In this study we choose α=0.4, lies closest to the observed experimental signal*.

AEXX	Signal [cm^{-1}]
0.2	16026
0.25	17091
0.3	18204
0.35	19390
0.4	20632
0.5	23390
Exp.	20408

S7: XRD spectra of the materials

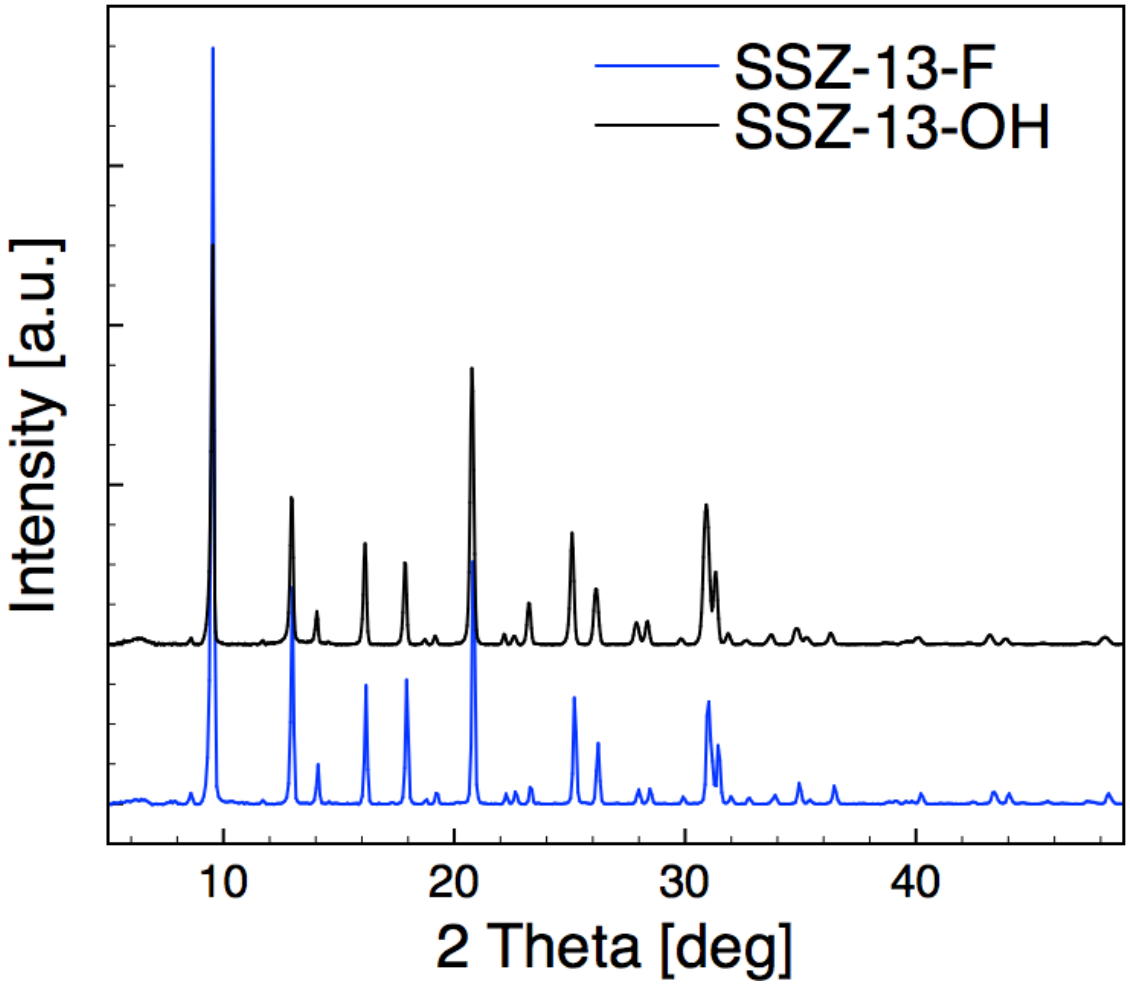

Figure S9: XRD spectra of SSZ-13-OH (black line) and SSZ-13-F (blue line) after synthesis.

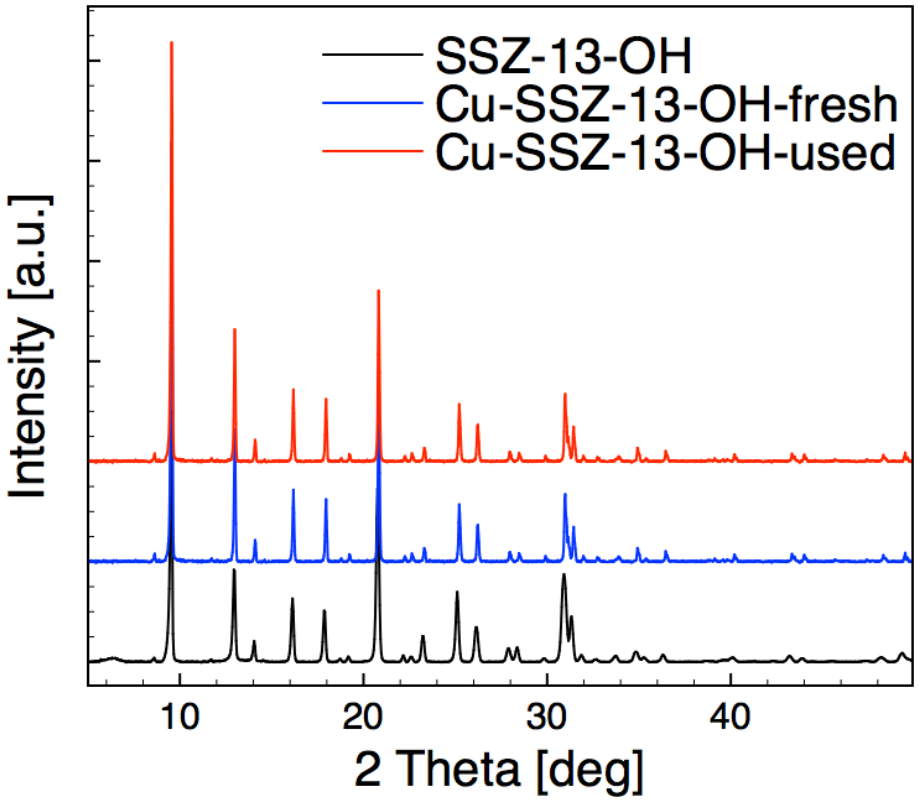

Figure S9: XRD spectra of SSZ-13 OH (black line) and Cu-SSZ-13-OH after ion exchange (Cu-SSZ-13-OH-fresh, blue line) and Cu-SSZ-13-OH after several treatment cycles (Cu-SSZ-13-OH-used, red line). We find that the framework structure remains intact.